

A STEREOLOGICAL STUDY OF DENSIFICATION OF POROUS METAL STRIP DURING ROLLING

A Thesis Submitted

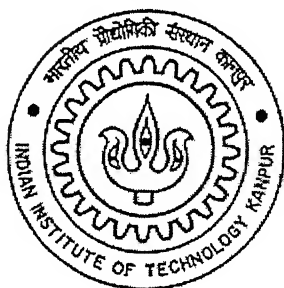
In Partial Fulfillment of the Requirements

For the degree of

Master of Technology

By

Vimal Kishor Jha
(Roll No. Y210632)



to the

DEPARTMENT OF MATERIALS AND METALLURGICAL ENGINEERING

INDIAN INSTITUTE OF TECHNOLOGY, KANPUR

JULY 2004

A STEREOLOGICAL STUDY OF DENSIFICATION OF POROUS METAL STRIP DURING ROLLING

A Thesis Submitted

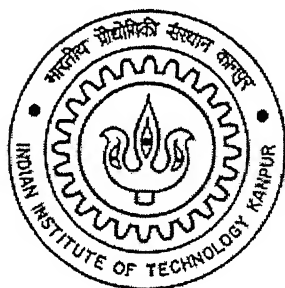
In Partial Fulfillment of the Requirements

For the degree of

Master of Technology

By

Vimal Kishor Jha
(Roll No. Y210632)

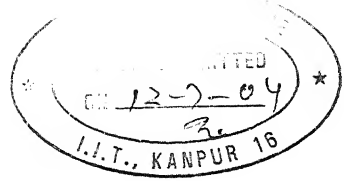


to the

DEPARTMENT OF MATERIALS AND METALLURGICAL ENGINEERING

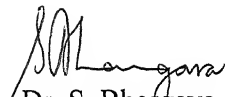
INDIAN INSTITUTE OF TECHNOLOGY, KANPUR

JULY 2004



CERTIFICATE

It is certified that the work contained in the thesis entitled “A Stereological Study of
Densification of Porous Metal Strip during Rolling” by Vimal Kishor Jha (Roll No.
Y210632), has been carried out under our supervision and to the best of our knowledge
this work has not been submitted elsewhere for a degree.



Dr. S. Bhargava

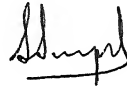
Professor

Department of Materials and

Metallurgical Engineering

Indian Institute of Technology

Kanpur



Dr. S. Sangal

Professor

Department of Materials and

Metallurgical Engineering

Indian Institute of Technology

Kanpur

25 OCT 2004

दुर्धरात्तम माधोनाथ केलकर पुस्तकालय
भारतीय प्रौद्योगिकी संस्थान कानपुर
भवापि ६० १४९२९५

TH
MMS/2004/10
J559.8



A149295

ABSTRACT

An understanding regarding the densification of porous metal preforms, as a function of rolling thickness reduction, can either be studied by generating the experimental data and fitting with an empirical relationship or can be analyzed by solving constitutive equations written for the plane-strain conditions that exist during rolling of a flat sheet. The present study gives micro-level description of densification rolling of a porous metal strip by studying the changes that take place in the surface area of pores per unit volume, average pore size, pore size distribution and aspect ratio of pores and grains with the help of Stereological concepts, which uses Image Analyzer as its main tool. In this study Ni powder was compacted through die compaction, then sintered and finally subjected to different amount of deformations by means of cold rolling, maintaining plain strain condition. The strip produced for different deformations has been analyzed for the variation in the internal structure of the Ni strip during densification rolling.

ACKNOWLEDGEMENTS

At the outset I would like to convey my deepest sense of gratitude to my thesis supervisors Dr. S. Bhargava and Dr. S. Sangal for their expert guidance and continuous encouragement throughout the course of my work. Their guidance, intellectual support and creative criticism lead the work to success.

I am very thankful to Mr. Manoj Kumar, Mr. Anand Rao, Mr. Rajeev Kumar and Mr. Debjyoti Maitra for helping me in sorting out both experimental and theoretical problems I faced during this work. I would like to convey my sincere thanks to Mr. Kumar and Mr. Bajpai for extending all possible and sincere help through out the course of my work

I must acknowledge the support provided by my beloved parents, brothers and sister. I would not have come this far without their unconditional love and support. This thesis is dedicated to them.

At last I would also thanks to anyone and everyone who directly or indirectly supported me in building up my carrier and made my stay at IIT Kanpur memorable

Vimal Kishor Jha
IIT Kanpur
July, 2004

TABLE OF CONTENTS

Page No.

Chapter 1.	Introduction	1
Chapter 2.	Literature Review	4
2.1	Powder metallurgy routes based on roll compaction of cold metal powder	6
2.1.1	Preparation of green strip	6
2.1.1.1	Direct metal powder rolling	
2.1.1.2	Effect of powder characteristics	13
2.1.1.3	Effect of processing parameters	16
2.1.2	Bonded metal powder rolling	21
2.2	Sintering	23
2.3	Densification of sintered strip	23
2.3.1	Repeated cold rolling and sintering /annealing cycle	24
2.3.2	Hot rolling	25
2.4	Final Cold Rolling and Annealing	28
2.5	Plasticity theory for porous metals	29
2.6	Analysis of the plane-strain cold densification rolling of a sintered porous metal strip by the upper-bound technique	29
2.6.1	Influence of rolling parameters	31
2.6.1.1	Friction factor	31
2.6.1.2	Percentage reduction	31
2.6.1.3	Roll radius	32
2.6.1.4	Roll speed	33
2.6.1.5	Initial relative density of the strip	35
2.7	Objective of the present work	36
Chapter 3.	Experimental Procedure	39
3.1	Raw material	39
3.1.1	Elemental nickel powder	39

3.2	Compaction	39
3.3	Sintering	39
3.4	Cold Rolling of Sintered Pellet	40
3.5	Quantitative Metallography	40
3.5.1	Specimen Preparation	40
3.5.2	Microstructural Studies	40
3.5.2.1	Volume fraction of Pores	41
3.5.2.2	Average Pore size	41
3.5.2.3	Aspect ratio of Pores	
3.5.2.4	Surface Area per unit Volume of pores(S_V)	42
3.5.2.5	Contiguity of Solid-Solid contact	42
3.5.2.6	Aspect ratio of grains	43
3.6	Scanning Electron Microscopy	44
Chapter 4.	Experimental Results	45
4.1	Starting material	45
4.2	Densification behavior	55
4.2.1	Effect of cold rolling reduction on volume fraction of pores	55
4.2.2	Effect of cold rolling reduction on surface area of pores per unit volume	56
4.2.3	Effect of cold rolling reduction on contiguity of solid-solid Contact	57
4.3	Morphology of Pores	57
4.3.1	Effect of cold rolling reduction on aspect ratio of pores	57
4.3.2	Effect of cold rolling reduction on average pore size	58
4.3.3	Effect of cold rolling reduction on aspect ratio of grains	59
4.3.4	Effect of cold rolling reduction on pore size distribution	60
Chapter 5.	Discussions	66
5.1	Effect of relative density of the strip on average pore size	66
5.2	Effect of relative density of the strip on surface area of pores	

	per unit volume	67
5.3	Effect of relative density of strip on aspect ratio of pores	68
5.4	Effect of relative density of strip on aspect ratio of grains	68
5.5	Effect of relative density of strip on contiguity	69
5.6	Conformance with the Koval'chenko equation	71
Chapter 6.	Conclusions	73
Chapter 7.	Suggestions for future work	74
Appendix A		75
Appendix B		79
References		80

LIST OF FIGURES

	<i>Page No.</i>
Figure 2.1. Typical roll positions for roll compaction of powders[25].	7
Figure 2.2. Typical arrangement for supplying metal powder into roll gap by saturated feed system.	7
Figure 2.3 Typical arrangement for supplying metal powder into roll gap by unsaturated feed system.	8
Figure 2.4. Forced feeders.	9
Figure 2.5. Various zones and angles in direct metal powder rolling.	9
Figure 2.6 Variation of green strip density with compacting roll gap and roll speed [19].	13
Figure 2.7. Variation of green strip thickness with compacting roll gap and roll speed.[19].	15
Figure 2.8. Variation in strip density with roll speed for MH100 iron powder at various indicated roll gaps [1].	17
Figure 2.9. Schematic diagram showing effect of roll diameter on amount of powder pulled into rolling gap.	18
Figure 2.10. Transverse density distribution in green strip.	20
Figure 2.11. Effect of cold rolling reduction on tensile properties (post annealed) of sintered stainless steel strip.	25
Figure 2.12. Efficiency of densification of sintered steel strip versus final density for single pass hot rolling at different relative density of sintered strip[9].	27
Figure 2.13. Effect of relative density of porous copper strip on apparent plastic Poisson's ratio during hot rolling[7].	28
Figure 2.14. Effect of the friction factor on the densification and power.	31
Figure 2.15. Effect of the friction factor on the percentage slip.	33
Figure 2.16. Effect of the thickness reduction on the densification.	34
Figure 2.17. Effect of the roll radius on the densification and the power.	34
Figure 2.18. Effect of the roll speed on the densification and the power.	35

Figure 2.19. Effect of the initial strip thickness on the densification and the power.	36
Figure 3.1. Superimposing grid on a Micrograph for calculation of Contiguity ratio.	44
Figure 3.2. Superimposing grid on a Micrograph for calculation of volume fraction of particular phase.	44
Figure 4.1 Optical Micrograph at 0% cold rolling reduction.	45
Figure 4.2. SEM of the fracture surface of the metal strip at 0% cold rolling reduction.	46
Figure 4.3. Optical Micrographs of the metal strip at (a) 20% and (b) 25% cold rolling reductions.	47
Figure 4.4. Optical Micrographs of the metal strip at (a) 30%, (b) 35%, (c) 40%, (d) 45% and (e) 50% cold rolling reductions.	49
Figure 4.5. Optical Micrographs of the metal strip at (a) 55% and (b) 60% cold rolling reductions.	50
Figure 4.6. Optical Micrograph of the metal strip at 65% cold rolling Reduction.	51
Figure 4.7 SEM of the fracture surface of the metal strip at 40% cold rolling reduction.	52
Figure 4.8 SEM of the fracture surface of the metal strip at 45% cold rolling Reduction.	53
Figure 4.9. SEM of the fracture surface of the strip at 55% cold rolling Reduction.	54
Figure 4.10. Effect of cold rolling reductions on volume fraction of pores. Error bar is representing the 95 % CL.	55
Figure 4.11. Effect of cold rolling reductions on Surface area of pores per unit volume. Error bar is representing the 95 % CL.	56
Figure 4.12. Effect of Cold Rolling reduction on Contiguity of solid-solid Contact.	57
Figure 4.13. Effect of Cold Rolling reduction on Aspect Ratio of Pores.	58
Figure 4.14. Effect of cold rolling reduction on the average pore size. Error	

bar is representing the 95 % CL.	59
Figure 4.15. Effect of Cold Rolling reduction on Aspect Ratio of Grains.	59
Figure 4.16. Pore Size Distribution Histogram for (a) 0%, (b) 20%, (c) 40%, and (d) 60% Cold Rolling reduction.	62
Figure 4.17. Pore size Probability distribution function on (a) 0%, (b) 20%, (c) 40% and (d) 60% Cold Rolling reduction.	64
Figure 5.1. Changes in average pore size with the changes in relative density of strip.	66
Figure 5.2. Changes in surface area of pores per unit volume with the changes in relative density of strip.	67
Figure 5.3. Changes in aspect ratio of pores with the changes in relative density of strip.	68
Figure 5.4. Changes in aspect ratio of grains with the changes in relative density of strip.	69
Figure 5.5. Changes contiguity ratio of solid-solid contact with the changes in relative density of strip.	70
Figure 5.6. Comparison of experimental data with the data obtained from equation 5.1.	72

CHAPTER 1

INTRODUCTION

In view of many novel advanced materials, including nanostructured materials, being synthesized using the powder based approach, powder based routes for producing bulk materials have gained considerable importance in the recent times. Thus, powder based deformation processes such as powder rolling, powder extrusion, powder forging etc are the processes which have seen a tremendous development in last two decades. Among various bulk forms and shapes, thin strips find many engineering applications and have been produced on a commercial basis using powder as the starting raw material in several cases. In contrast to the ingot metallurgy (I/M) routes whereby a thin slab is continuously cast and is extensively reduced in thickness by a combination of extensive hot and cold rolling schedules, the powder metallurgy (P/M) routes consist of making a green metal strip by a variety of methods followed by sintering and hot/cold rolling. However, the requirement of imparting heavy thickness reductions to continuously cast slabs, so as to breakdown the cast structure, does not exist in powder-based routes for thin strip making. In contrast, requirements of imparting thickness reduction by hot/cold rolling to sintered porous metal strip, which is invariably a step in all powder-based routes for strip making, arise due to the need of eliminating porosity so as to get a fully dense metal strip. Working out an engineering process flow chart for such processes therefore requires predicting the minimum thickness reduction required to fully densify a porous metal strip of the given starting relative density.

The interest in understanding densification in powder-based deformation processes also arises from the fact that pore elimination mechanisms existing in such processes are fundamentally different than that in other full-densification processes such as hot isostatic pressing (HIP'ing). It is to be noted that while the stress field applied in a process such as hot isostatic pressing consists of the hydrostatic component alone, those applied in powder deformation processes comprise of not only hydrostatic stress component but also deviatoric stress component. Therefore, while pores are expected to shrink without any shape change in processes such as hot

isostatic pressing they are expected to undergo shrinkage as well as shape change in powder deformation processes due to the presence of the deviatoric component in the applied stress field. An infinite pressure would be required to completely close a pore in isostatic pressing unless the elimination of pores is expected to occur by high-temperature time dependent diffusion assisted flow of matter. In contrast, due to the mechanism of elongation (shape change) followed by patching up of opposite surfaces of collapsing pores, the full densification in a porous preforms by powder deformation processes can occur by applying finite stress field without taking recourse to mechanisms related to high-temperature time dependent flow of matter. Powder deformation processes thus can be effectively used to consolidate sintered porous mass obtained from powders that have non-equilibrium phases or have amorphous/nano-crystalline structure.

An understanding regarding the densification of porous metal performs, as a function of rolling thickness reduction, can either be studied by generating the experimental data and fitting with an empirical relationship or can be analyzed by solving constitutive equations written for the plane-strain conditions that exist during rolling of a flat sheet. Efforts have also been made to generate such an understanding by analyzing densification of porous material using the finite element method (FEM) approach. A micro-level description of densification rolling of a porous metal strip, however, requires an understanding of the changes that take place in

- (i) The free surface area of particles
- (ii) The average coordination number and the average contact area per particle
- (iii) Average pore size and aspect ratio
- (iv) Shape of particles, and
- (v) Shape of pores.

Empirical approach as well as the approach based on stress-strain analysis, though giving satisfactory engineering solutions, fail to generate the basic micro-level fundamental mechanisms of pore removal and changes that occur in other micro-level

structural parameters of the porous metal strip during densification rolling. Stereology is a collection of mathematical methods that relate the parameters defining a spatial structure to lower dimensional measurements made on sections through the structure. Variation in the parameters such as grain size distribution, pore size distribution, surface area per unit volume of pores, mean grain size, contiguity and aspect ratio of pores/particles which can be conveniently measured by stereological analysis. Very limited observations regarding densification rolling of a porous metal strip using stereological analysis have, however, been reported in the literature.

The present study was undertaken to fill this gap. Porous nickel strips were prepared and were subsequently subjected to cold densification rolling for different thickness reductions. Results obtained through stereological observations have been described.

In our study Ni powder is being compacted by die compaction, then sintered and finally subjected to different amount of deformation by means of cold rolling maintaining plain strain condition.

CHAPTER 2

LITERATURE REVIEW

The making of metal strip by the PM technique involving roll compaction was first accidentally noted by Henry Bessemer in 1843, when he was trying to make brass flakes for pigment purposes from brass powders by feeding them into a rolling mill. Henry Bessemer did not pursue this work, and it was not until 1902 that a patent application for making tantalum strip from powder was filed in Germany and was granted to Siemens and Halske[2]. A patent was also issued to Hardy, in 1938 for rolling metal powders transported through the rolls of a horizontal mill on a carrier. The real stimulus to develop roll compaction of powders for making metal strip came only after the publication of classic paper by Naeser and Zirm[31] in 1950, in which they described a powder rolling process for making iron strip from iron powders. The Sylvania Electric products Corp. and the US Atomic Energy Commission did some of the powder rolling of many metals used in atomic reactors. Evens and Smith[30] at the University of Cambridge and Franssen in Germany showed that copper powder can also be processed into strip in a similar manner. A detailed evaluation of the process was published in 1959. One of the important landmarks in the history of roll compaction came in 1954 when Sherritt Gordon Mines in Canada started producing hydrometallurgical nickel and cobalt powders on a commercial Scale. Later Lund at the University of British Columbia in 1958 demonstrated that the hydrometallurgical nickel powder produced at the Sherritt refinery could be roll compacted and successfully processed into fully dense strip. The engineering and economic aspects of the process started attracting attention from research workers in the late 1950s. Smucker in 1959, reported his attempt, perhaps the first one of its kind, to use hot rolling as a means of densification of roll compacted and sintered copper and nickel strip at E. W. Bliss and Co., USA. The interesting feature of his approach was that the roll compaction unit, sintering furnace, and hot rolling mill were interlinked with each other and a continuous operation was possible. In the late 1950s the Republic Steel Corp., USA developed a process for making directly reduced iron powder cheaply. In

1959, they announced the successful operation of 50 mm wide low carbon steel strip from iron powder in a pilot plant operation. They also used hot rolling as a means of densifying roll compacted and sintered strip. Their results were published in 1962. Since Lund's work Sherritt Gordon Mines did considerable research and development (R&D) work in developing the process for making nickel and cobalt strip on a commercial scale, and finally started producing these strips in 1961. They used hot rolling as a means of densifying the roll compacted and sintered strip on a high speed batch basis. Their results were published during 1964-66.

It was clearly recognized that the success of the roll compaction depended on the availability of cheap metal powder. During the early 1960s, work on producing metal powder cheaply by various techniques was in progress. This added fresh impetus to R & D activities related to roll compaction. The British Steel Corporation started investigating further the roll compaction technique for making stainless steel strip at their Sheffield laboratory. At their Swansea laboratory BSC pioneered a new PM route based on roll compaction of bonded metal powder in the form of a coherent and flexible strip, which overcame many difficulties associated with the roll compaction of loose powder. During the same project, Tundermann and Singer at University College of Swansea, UK, carried out a detailed and systematic investigation on the various aspects of roll compaction, and their results were published in 1968-69. The International Nickel Co. investigated roll compaction for making porous nickel strip for battery and fuel cell electrode applications.

Around 1970 Singer at the University College of S started his efforts in developing routes for making metal strip based on the integration of the powder production by inert gas atomization of liquid metals with the subsequent consolidation processing step which led to the development of 'Spray rolling'. This process avoided the use of metal in the form of powder but instead used liquid metal droplets formed just after atomization without allowing them to solidify in powder form. Subsequently, Singer and co-workers extended the above concept of strip making using centrifugal spray deposition. Aurora Steels Ltd, Sheffield, developed

the full commercial scale 'Controlled s deposition' process, primarily for tool steels in various forms including sheet and strip. Research and development work were also underway by Cavanagh and Hollingberry at the Ontario Research Foundation in Canada and by Singer and Dube[28][29] at the University College of Swanssea, to develop routes for making metal strip based on the integration of powder production by gaseous reduction of high purity oxide powder derived from ores with subsequent consolidation processing. This led to the development of the 'Direct steel process' and the 'Direct strip process'. Dube in 1981-82[26][27] reviewed the roll compaction and related routes for making metal strip.

2.1 Powder metallurgy routes based on roll compaction of cold metal powder

The overall processing of metal powder into finished strip by PM routes based on the rolling of cold metal powder consists of the following unit operations:

1. Preparation of 'green' strip from metal powder.
2. Sintering of the green strip.
3. Densification rolling of the sintered strip
4. Final cold rolling and annealing.

2.1.1 Preparation of green strip

The first step in the PM method of strip making is the preparation of green strip, which may be defined as a mechanically bonded metal powder defined as a mechanically bonded metal powder formed into a strip which is relatively porous and brittle. This step may be carried out in two ways: direct metal powder rolling and bonded metal powder rolling.

2.1.1.1 Direct metal powder rolling

The original and most obvious way for making green strip is by supplying cold metal powder into the roll gap of a specially designed powder rolling mill, where the powder is subjected to sufficient pressure to form a self-supporting green strip. This method is generally known as direct metal powder rolling. The powder flow may be either horizontal or vertical. The vertical. The mill is preferred because this avoids

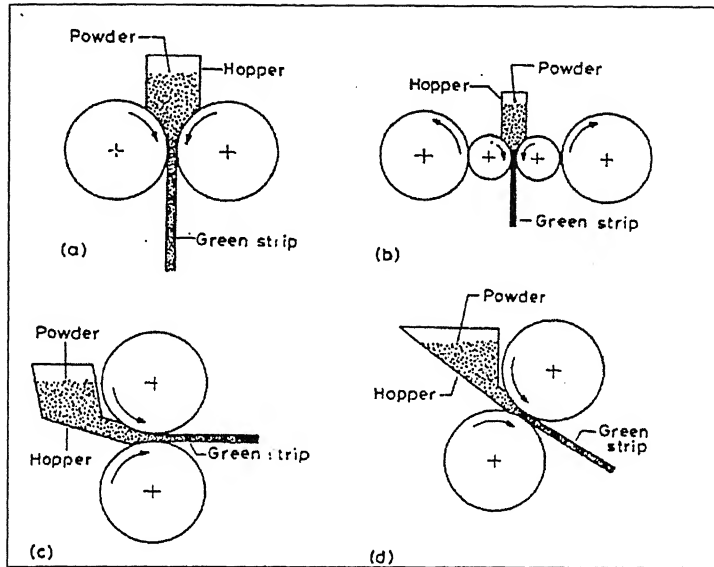


Figure 2.1. Typical roll positions for roll compaction of powders[25]

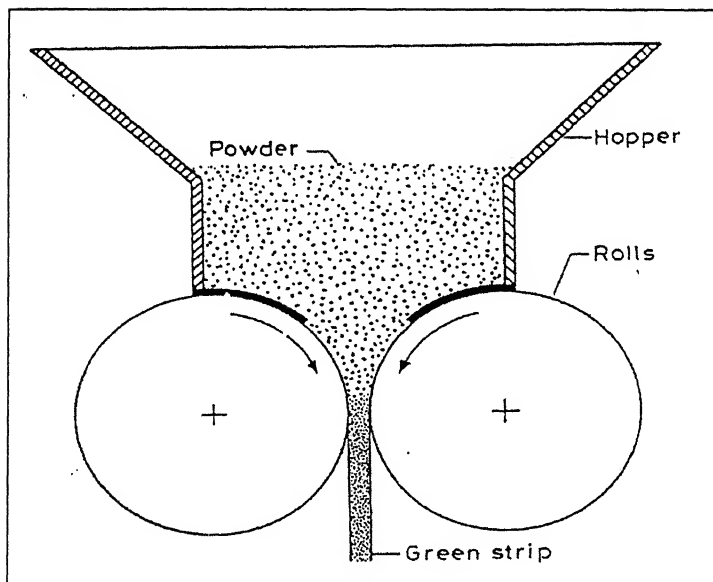


Figure 2.2. Typical arrangement for supplying metal powder into roll gap by saturated feed system.

the difficulty of feeding loose powder into the roll gap. Mills having rolls in an angled position have also been used in a few cases, but they are of academic interest only. The mill is usually of 2-high type but could be 4-high especially when the rolls are of small diameter. Typical roll positions are shown in Figure 2.1.

There are two basic methods of supplying metal powder to the roll gap: saturated feeding, unsaturated feed system. In saturated feeding, an excess amount of powder is fed to the nip of the rolls (Figure 2.2) and therefore the amount which passes through the mill is controlled by

- a) The frictional forces existing between the powder and roll surface, and between the powder particles themselves, and
- (b) The flow properties of the powder. The head of powder in the hopper should be held constant for obtaining constant density along the strip length.

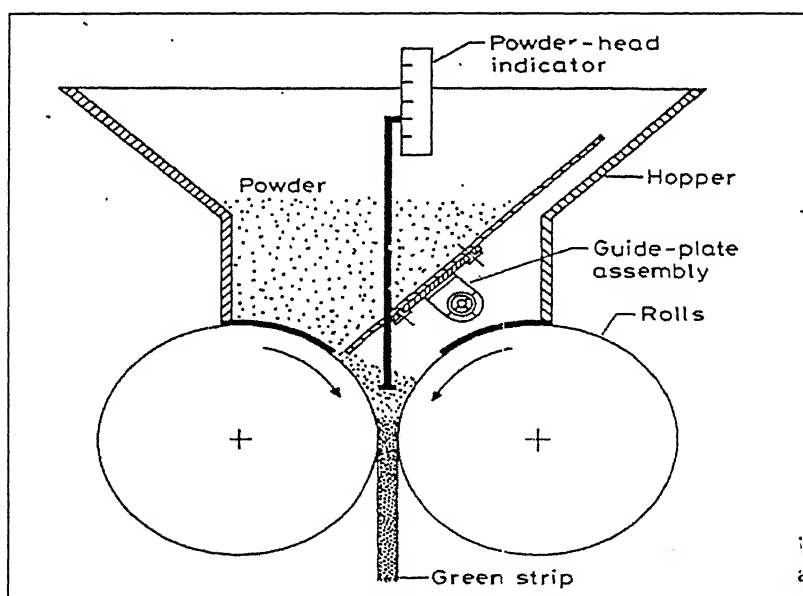


Figure 2.3. Typical arrangement for supplying metal powder into roll gap by unsaturated feed system.

The unsaturated method of feeding powder differs from the above method in that a metering device is used to regulate the amount of powder being fed. The fed is

proportioned with an adjustable guide plate, which controls the opening of the feeding section. A typical method of unsaturated feeding is shown in Figure 2.3.

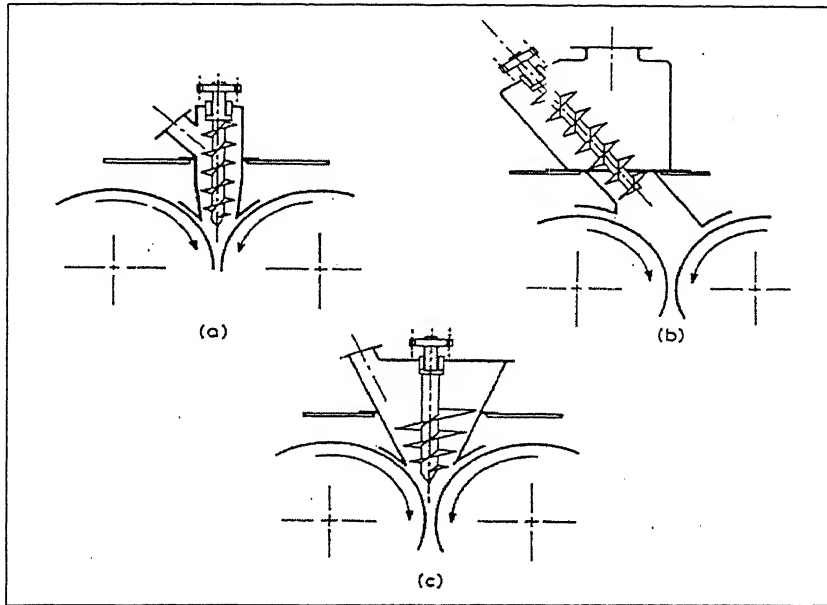


Figure 2.4. Forced feeders

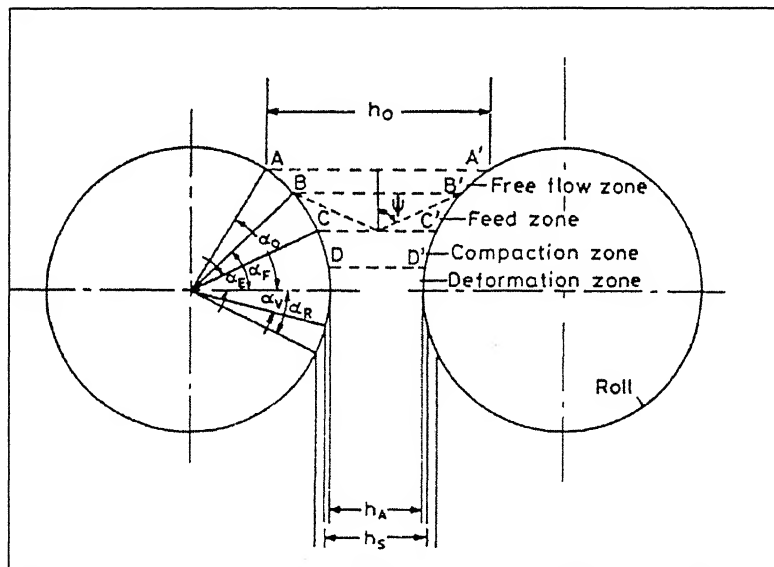


Figure 2.5. Various Zones and angles in direct metal powder rolling

The unsaturated feed system leads to considerable control difficulties with direct powder rolling. The saturated feed system also fails to produce the desired result, but is more stable and capable of providing acceptable strip at very low line speeds. A variation on both these feeding methods is that of forced feeding. See Figure 2.4, where a mechanical device, such as a screw, is used to increase the feed rate above that possible by gravitational forces

The roll bite in vertical, saturated powder rolling can be broadly divided into four zones, not clearly distinguishable, through which the powder mass passes, as shown in Figure 2.5:

- (i) Free flow zone: in which powder falls under gravity
- (ii) Feed zone: in which the powder, though remaining non-coherent, is being dragged down by the friction on the roll surface. Densification depends solely on the rearrangement of particles. The density of the powder mass reaches maximum density at the end of the zone. The feed zone is defined by two angles α_F and α_E . The corresponding angle of starting feed position B or B' on the roll surface is called the feed angle α_F .
- (iii) Compaction zone: within which the rolling force becomes effective and the powder mass becomes coherent. The start of this zone is defined by the angle of compaction, grippign angle, angle of rolling, or angle of grip α_E .
- (iv) Deformation zone: where deformation of powder takes place. It is believed that the green strength of the outgoing strip is primarily developed in this zone. This zone often overlaps with the compaction zone.

Angle of delivery α_0 is the angle corresponding to the width h_0 of the feed opening above the rolls, as shown in Figure 2.5. α_v is the angle of elastic compression of the rolls, which determines the thickness h_s of the compacted strip. α_v would be

the elastic deformation of the rolls could be ignored. However, in most cases the compacted strip is even thicker than h_s because of the elastic recovery of the compacted powder mass. The angle corresponding to the actual outlet plane is known as angle of release α_R , as shown in Figure 2.5. For most metals, the angle of grip was found to be about 7° . However, it depends on the shape of the powder. Expressions for the gripping angle have been derived by Smucker[5], and Lee and Schwartz[24].

The entrainment of the powder into the compaction zone depends on the feed angle and gripping angle, and since these angles depend on the coefficient of friction μ , any increase in μ will increase the compaction zone. Thus for a given compaction ratio, the thickness of the strip increases as the coefficient of friction increases. The most important factors likely to affect the roll/rolls, the temperature of rolling, and powder morphology. Evans and Smith[2][23] obtained a copper strip 100% thicker when the mirror polished rolls were roughened by sand blasting. Similarly, the thickness of the strip was increased by 25% when copper powder was heated in inert atmosphere to 573 K before being fed into the roll gap. The rolling of hot powder is discussed below. Clegg et al. observed that the thickness and density of the nickel strip prepared from atomized nickel powder were, respectively, about 33 and 0.6% greater than those prepared from annealed hydrometallurgical nickel powder. The greater thickness was attributed primarily to different particle morphologies resulting in higher antiparticle and roll/particle friction coefficients.

Tundermann and Singer[1] observed that there is a relative movement of powder particles during roll compaction. They observed, using electrolytic iron Elec 100 powder particles, that roll compaction leads to higher strength in the green strip than in strip prepared by die compaction. Such movement under any condition is affected greatly by particle shape. In the case of extremely irregular MH 100 sponge from powder, they did not observe much difference in the strength of roll compacted and die compacted green strip. Kimura et al. concluded that the compacting efficiency is greater in powder rolling than in die compaction, because of less loss of pressure by the friction of die walls and buffering by occluded air in the die mould.

Lund[19], in the case nickel powder, observed that very little plastic deformation of the powder particles occurs in the roll compaction operation. On the other hand, Blore et al[11]. observed that only the powder particles on the surface of the compacted strip are seen to be appreciably deformed. However, no quantitative assessment was done by these workers. On the basis of microhardness measurements, Tundermann and Singer[22] showed that the maximum amount of bulk deformation in the case of rolling iron powder to ~91% relative density is about 12-15%. The particle deformation was found to be related to strip density. In the case of iron, it increased sharply at densities above $-6.6 \times 10^3 \text{ kg m}^{-3}$ no appreciable deformation occurred. Blore et al[11]. reported that the transverse tensile strength of green nickel strips is about 20% less than the longitudinal strength, and it seems that there is preferentially more deformation in the longitudinal direction than in the transverse direction. Tundermann and Singer[22] while contradicting the claims of Evans and Smith' on particle deformation demonstrated that for iron as for copper, the powder particles are slightly elongated in the rolling direction and compressed in the rolling plane. Clegg et al[21]. in their work on nickel powders of different morphologies showed that the amount of hardening induced in powder particles hydrometallurgical nickel powders, which had a higher hardness than atomized nickel powder, are interlocked but unreformed, while the particles of the latter are deformed and moulded against each other.

In the initial region, the main cause of densification is believed to be the restacking of the powder particles brought about by vibration and very limited compacting forces. Such restacking involves very little plastic deformation. At higher pressures, i.e. beyond restacking zone, localised deformation, fragmentation, and plastic deformation of the particles occur and cause further restacking and densification. Smirnov et al[4]. observed that particle rotation occurs during metal powder rolling, while powder sliding occurs during pressing. This view is supported by the results of the experiments of Atkinson, in which alternate layers of black and white material were passed through a pair of pocketed rolls. It was observed that the material does not move in horizontal layers but exhibited shear faults. The layers

which were originally horizontal above the point of entrainment appear as vertical layers in the compact i.e. a 90° rotation occurs. However, there was some evidence that this rotation occurred before any compaction commenced.

2.1.1.2 Effect of powder characteristics:

The powder characteristics of importance in direct powder rolling are size, shape, and size distribution; these control the flow properties of the powder. Coarse powders for the same mass. Hence strips produced from the fine powders for the same mass. Hence strip produced from fine powder are relatively stronger than those produced from large size powders. Lund's work[19] on the rolling of nickel powder shows that both the average density and thickness of the green strip increase as the

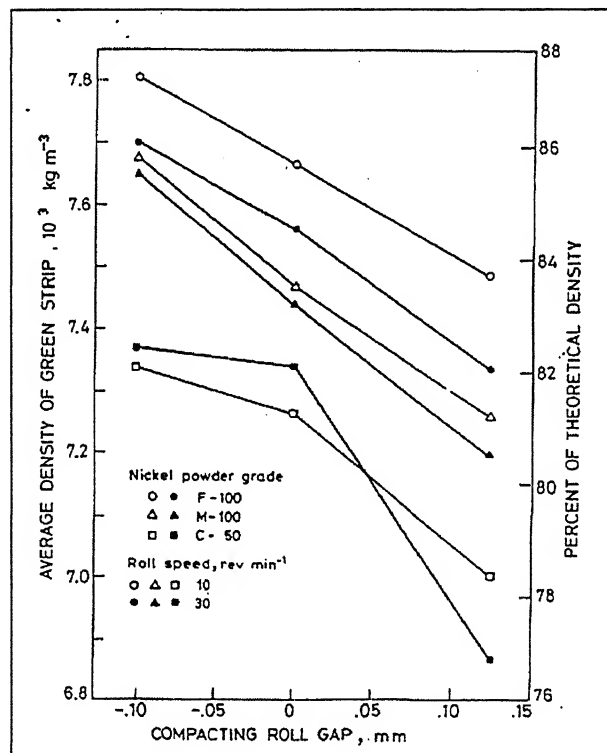


Figure 2.6. Variation of green strip density with compacting roll gap and roll speed [19]

average size of the powder decreases see Figure 2.6 and 2.7. The negative roll gap shown in the above figures was obtained by tightening the rolls beyond the point of

initial contact (i.e. zero gap). Contrary to this, Tundermann and Singer[1] observed that strip density and strength first increase and then decrease as particle size increases at a given roll speed. Their observation that these properties decrease as the roll speed increases is in agreement with that of Lund. Extremely fine powders do not bond properly.

The particle morphology and surface roughness strongly affect the flow and compaction. Spherical powders are more difficult to roll compact than irregularly shaped powders. Spherical powders have good flow properties but lack interlocking of particles during roll compaction, whereas irregular shape assists in interlocking of particles during roll compaction and imparts strength. Hunt and Eborall found that atomised nickel powder, which was spherical, could not be rolled successfully. The surface roughness or shape irregularity of the powders must not be increased unduly since the flowrate of the powder would decrease, which would produce a green strip of lower density, thickness, and strength. A compromise is usually struck between the interlocking factor and the flowability of powders. The particle morphology also plays an important role. It has been reported that water atomised nickel powder gave thicker strip on roll compaction than hydrometallurgical nickel powders. The former type of powder had a morphology ranging from spheroidal fine particles to irregular coarse particles, which resulted in higher interparticles and roll/particle friction coefficients, causing atomized particles to be drawn more readily into the roll nip. The particles hardness also plays an important role in achieving better mechanical properties of green strip. In the case of nickel, hydrometallurgical powder is harder than atomized powder. The green strip produced from atomized nickel powder was found to be denser than that from hydrometallurgical powder, because of greater deformation of the relatively softer atomized nickel powder during roll compaction.

The powder must flow at a rate that keeps pace property of the powder is of considerable importance. The flow behaviour of powders depends on size and shape, and also indirectly on the speed of rolling. Even the smallest addition of moisture is detrimental to powder flow. The effect of shape on powder flow has been discussed above. The effect of rolling speed is discussed below. Powders of low apparent

lensity have excessively low flowability, which leads to difficulty in feeding the powder to rolls, and roll compaction, if done at all, can be done only at a very low speed or alternatively using the forced feed system. The standard Hall flowmeter flow est does not provide a realistic means of assessing the powder flow behaviour in the rolling process, since it applies only to powder flow under a limited set of condition. Flowrates from hoppers with rectangular apertures give results that are more realistic with respect to the conditions found in powder rolling.

The presence of oxide film to powder particles creates a serious obstacle to cold bonding during strength. This problem can be overcome only by plastic deformation large enough to rupture the oxide film and enabling good metal-to-metal contact.

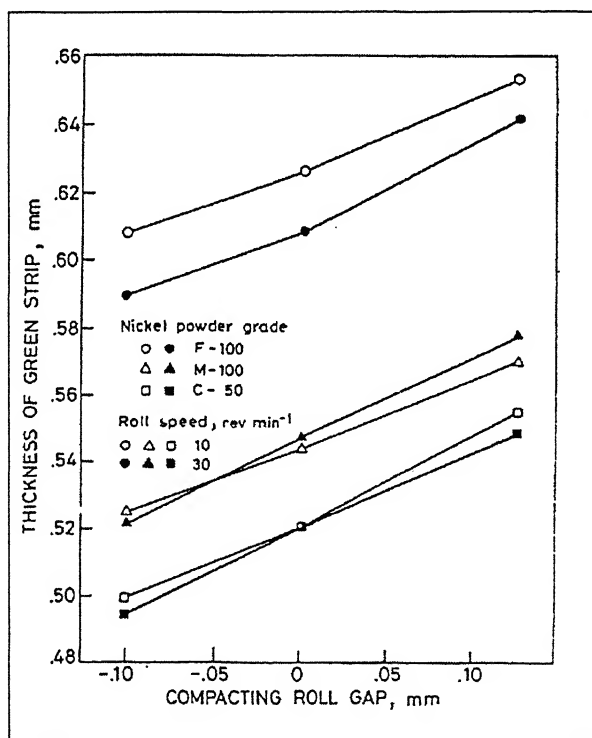


Figure 2.7. Variation of green strip thickness with compacting roll gap and roll speed.[19]

2.1.1.3 Effect of processing parameters

Increasing the roll gap increases the strip thickness but the density of the strip decreases so that only a moderate increase in mass flowrate is achieved[11]. Increase in roll gap alone will, therefore, produce low strength strip. Evans and Smith[3][2] found that for any given roll diameter there was a maximum roll gap above which coherent strip can not be produced. At very small roll gaps, strip densities greater than 90% of the theoretical may be produced, but edge cracking occurs as the strip exits from the rolls, and blisters form during sintering. The minimum roll gap setting is not well defined; in most cases it is taken as the point at which the issuing strip exhibits cracking at any given roll speed.

During rolling air is ejected which passes back through the powder mass and fluidises the powder feed and thereby restrict the powder flow. Fluidization increases. Thus, the effect of rolling speed should be considered in conjunction with the powder feed. Many investigators believe that at high rolling speeds the strip produced is of inferior quality, particularly of poor density of the strip as roll speed increased may be attributed in part to the shorter time for which each element of strip as roll speed increased may be attributed in part to the shorter time for which each element of strip length is subjected to pressure, and in part to a greater agitation effect on the powder caused by a higher velocity of escape entrapped air. The latter explanation is supported by the fact that if the rolling is carried out under gases such as hydrogen, having lower viscosity than air, then in addition to the strength, both the thickness and density of the strip are increased to such an extent that output can increase by 70%. Vinogradov and Fedorchenko observed that the use of vacuum in rolling removes the counterflow effect and increases interparticle friction and friction between the powder and roll surface. However, rolling under low viscosity gas or vacuum is not industrially attractive. Worn and Perks have reported that in the case of carbonyl nickel powder doubling the speed from 20 to 42 mm s⁻¹ results in only a minor improvement in production, e.g. ~ 15% increase at a powder head of 160 mm and a roll gap of 0.25 mm. This improvement was markedly less than might be expected. Further, the improvement was obtained only at the expense of the strength of green

strip. This adverse effect is caused by fluidisation of powder at higher speeds. There is practically no or very little change in density up to a certain speed. Tundermann and Singer investigated this point in detail and observed that at a given roll gap, the density and thickness of green strip remain constant up to a certain speed named the transition speed, the roll speed increases. The effect becomes more pronounced as the roll gap is reduced. Up to the flow transition speed, and thus density and thickness remain relatively constant during the linear flow-roll speed phase. Such a behaviour is shown in Figure 2.8. Powder flow properties and the evolution of air through the powder mass above the flow transition speed restrict the amount of powder compacted, and the density and thickness decrease. A forced feed technique seems to be more effective at high rolling speeds where the supply of the powder by a gravity feed can become insufficient to allow a coherent strip to be produced.

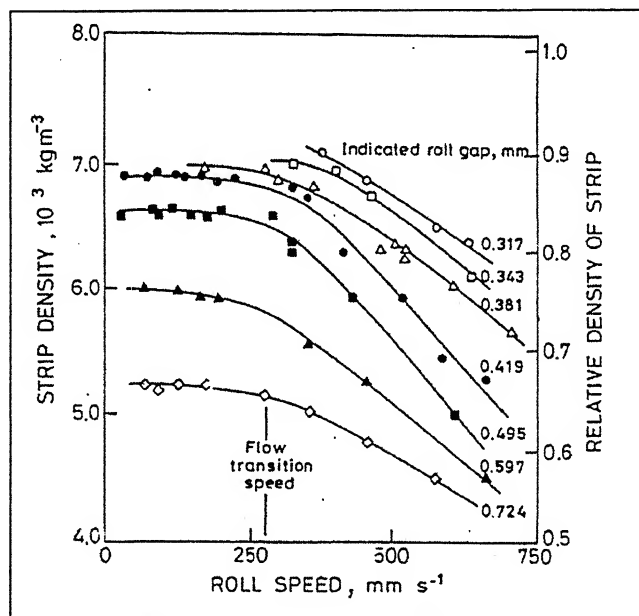


Figure 2.8. Variation in strip density with roll speed for MH100 iron powder at various indicated roll gaps [1]

Some workers have derived an expression for the theoretical maximum speed of roll compaction, and their values have been found to be in good agreement with

those obtained experimentally. The maximum rolling speed described is usually 0.05 m s^{-1} although speeds of 0.32 m s^{-1} with stainless steel powder, 0.38 m s^{-1} with copper powder, and 0.5 m s^{-1} with iron powder have also been reported.

Assuming that the rolls surface speed and other variables are the same, larger diameter rolls will produce a denser, and hence a higher, green strength, strip than the smaller diameter rolls. It can be seen from Figure 2.9 that for a larger diameter roll, a larger area is included by the angle of grip on the roll surface. Therefore, a larger amount of powder is pulled into the roll gap than for a smaller diameter roll. Assuming that there is no slip and distortion in the powder mass, and no spread occurs, the following equation gives a relationship between roll diameter D and the porosity E_{\min} at the narrowest point, i.e. of the out coming strip

$$\varepsilon_{\min} = 1 - \frac{\rho_t [D(1 - \cos \alpha_E) + h_A]}{\rho h_A} \quad (2.1)$$

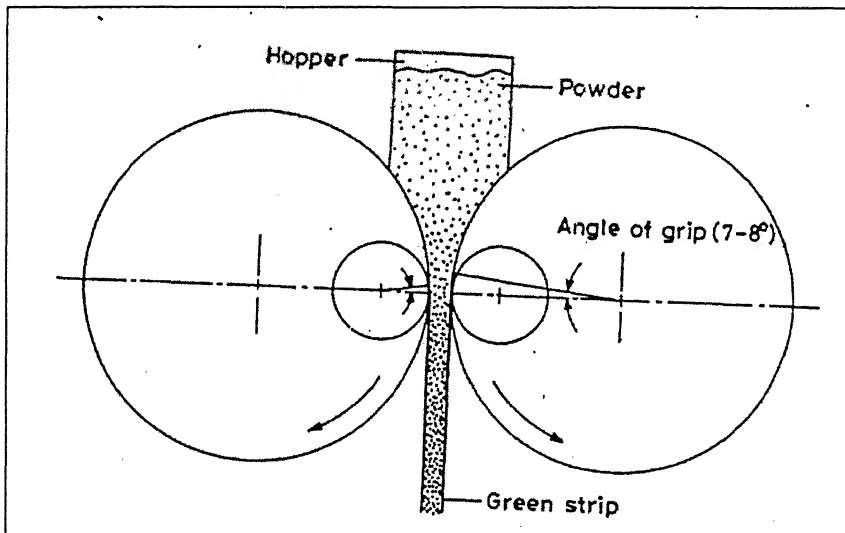


Figure 2.9. Schematic diagram showing effect of roll diameter on amount of powder pulled into rolling gap.

Where h_A is the roll gap, α_E the compaction angle, ρ_t the tap density of the powder. Shima and Yamada[20] used an upper bound theorem for predicting the thickness and density of the green strip. However, the theoretical values of density

and thickness at higher speeds may differ from the experimental ones, because of the fluidisation problem. It has been observed that the maximum green strip thickness is proportional to the roll diameter and varies from 0.33 to 1.0% of the roll diameter, depending on the type of powder. Moreover, with larger diameter rolls one can handle coarser particles and can produce thicker strip.

Lund[19], in his work on the rolling of nickel powder, found that within the range of green strip density $6.9 \times 10^3 - 7.8 \times 10^3 \text{ kg m}^{-3}$, the powder size, roll gap, and roll speed are relatively unimportant in terms of the quality of the finished product. However, the various powder and process parameters are important as far as the production of satisfactory green strip is concerned.

The green strip has an appearance like that of a metal strip with a matte finish. This strip is not fully dense, usually containing 10-20% porosity, which is not all open to the outside atmosphere; about half the green strip, which depends on the density and powder morphology is very low, and the elongation is virtually zero. For example, in the case of atomized nickel the tensile strength of the green strip is about 0.8 MN m^{-2} at a density level of 88% of the theoretical, while this can be increased five-fold even at a relative density level of 77% if the hydrometallurgical nickel powder is used, which has superior interlocking characteristics during roll compaction resulting from 'berry' and 'cauliflower' type shapes. The mechanics of roll compaction have been studied by many workers, and the forward slip, relative densification in the forward slip zone, distribution of roll pressure along the are of contact, and the final strip thickness have been calculated. The control of density in the green strip is an important factor in powder rolling. Tundermann and Singer's work demonstrated that there is very little variation (of the order of $\pm 1\text{-}2\%$ at 95% confidence limit) in density in the length direction, provided a scraper is used to remove any loose particles carried over by the roll so as to keep the roll surfaces clean. Their work also shows that the density variation across the strip thickness is symmetrical about the center of the strip, and the density is higher in the center relative to the surface of the strip for densities above $\sim 70\%$ of theoretical. However, the difference between the density at the strip surface and center decreases as the

overall strip density increases, and hence as the strip thickness decreases. A major problem encountered in the direct powder rolling has been the control of density distribution across the width of the strip. Because of powder leakage from both sides of the strip, coupled with reduced flowrate near the edges of the roll because of friction between hopper plate and powder, a parabolic density distribution is found across the width of the strip (Figure 2.10). Such strip has very weak edges, leading to handling problems and low yield in the green state. Moreover, considerable problems arise during the subsequent processing of such strips. A considerable amount of R&D work has been carried out in the area of controlling the density across the width of the green strip. This problem can be overcome by the use of appropriate edge restraints, such as a pressure plate or shoe against the opening, box shaped roll passes, flanges in the roll corners, loops and belts running on the rolls, etc.; some of these are shown. All the methods are aimed towards keeping the powder in place during its passage. A radioactive technique to measure the mass per unit area of the green strip and a mechanical measuring device to measure strip thickness.

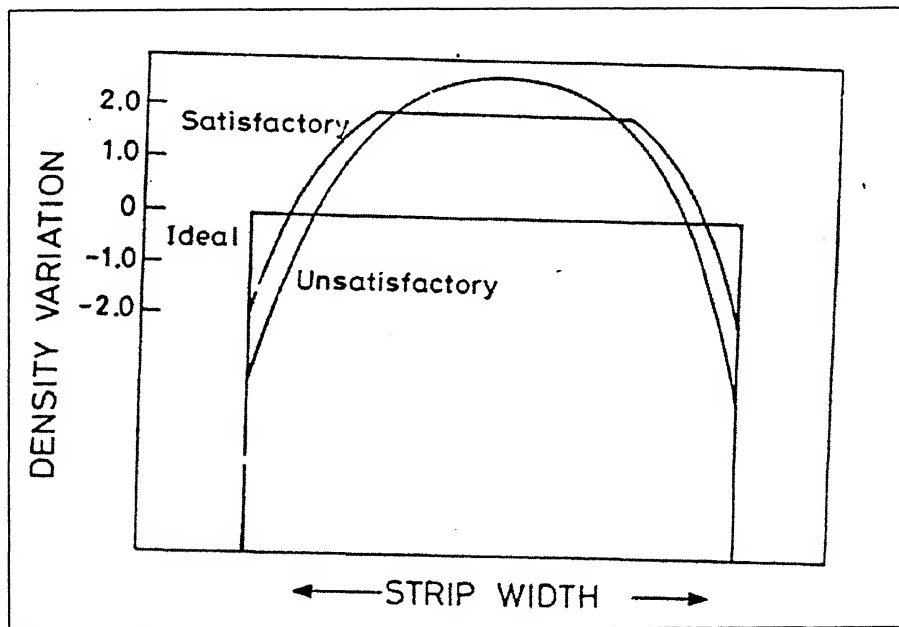


Figure 2.10. Transverse density distribution in green strip.

1.1.2 Bonded metal powder rolling

Feeding bonded metal powder into the roll gap in the form of coherent strip can overcome some of the problems of the form of coherent strip can overcome some of the speed and metering problems and lack of green strip flexibility experienced in direct metal powder rolling. This coherent strip enables the feeding of accurately metered quantities of powder into the rolling mill. The preparation of green strip by this method consists of the following basic steps:

1. Preparation of a slurry mixture from metal powder, a binder, a solvent, and sometimes, depending on the nature of binder, a plasticiser.
2. Deposition of the slurry on a substance.
3. Drying of the slurry on the substrate, which after removal from the substrate yields a coherent and flexible strip.
4. Densification of the dried strip by roll compaction.

A solvent should have essentially the following characteristics: low boiling point, low viscosity, ability to dissolve binder and plasticiser, and no reactivity. Solvents offer these advantages but suffer from such disadvantages as their high cost, high toxicity, and flammability hazards. Water, on the other hand, is cheaper and non-toxic but has a relatively higher boiling point. The purpose of the binder is to provide sufficient strength to green dry strip after the solvent has evaporated. The binders are dissolved molecularly in water or an organic solvent, or are dispersed in liquid as an emulsion. Organic binders strongly affect the rheology of the liquid phase, and increase the viscosity of the solvent, and also change the flow characteristics in most cases. The applicability of a green organic binder is very much dependent on the rheological characteristics of the binder solution. A binder, in general, should satisfy the following requirement.

1. It should form a solution of sufficient viscosity at low concentrations and should be available in a wide range of viscosity grades.

2. It must form a coherent self-supporting film when dried out, and should act as lubricant during roll compaction.
3. It must be readily removed during the sintering operation and should not leave any undesirable residue.

After drying, binders often become hard and stiff. Therefore, plasticizers are added which make the binder soft in the dry or near dry state. Plasticizers are lower molecular weight organic compounds, which dissolve in the same liquid as the binder. The plasticizer helps in disrupting the close aligning and bonding of the binder molecules, and it increases the flexibility of the green strip.

It is necessary that the metal powder-binder solvent slurry has sufficient viscosity for the metal powder to be sufficiently stable in suspension to permit the formation of a slurry that remains substantially homogeneous over a period of time. On the other hand, the viscosity should not be so high as to impair the flow properties of the slurry. It has been reported that with the use of Celacol binder the viscosity of the slurry can be varied between 100 and 1 N s m⁻² to suit the deposition method employed. The relative proportion of metal powder in binder solution depends on the size of powder.

On the laboratory scale, a simple doctor blade system[18] has been employed to deposit slurry on a moving substrate such as continuous stainless steel belt. The speed of operation was low, of the order of 2 mm s⁻¹, as ribbing streaking of the deposit occurs at a higher speed of the order of 400 mm s⁻¹. However, the slurry viscosity suitable for roller coating is in the 1-5 N s m⁻² range, and it is necessary to maintain a constant action at these lower viscosities to avoid setting out of the powder.

The time for drying of the deposited slurry depends mainly on the thickness of the deposit. It has been claimed[17] that the drying of an aqueous iron slurry deposit can be compacted in 30s by heating through the substrate, although the thickness of the deposit is not mentioned. A cold air draught is usually passed over top of the coating to remove water vapour and to prevent boiling. The dried strip is coherent and

can be handled. After removing the dry strip from the substrate it is rolled to increase its density and hence strength.

2 Sintering:

The green strip produced by roll compaction is relatively porous, containing typically 15-20% porosity, and has comparatively little strength and ductility. The strip is sintered at suitable temperatures to improve the physical and mechanical properties. The main aim in carrying out the sintering operation is to impart sufficient strength and ductility to the green strip to permit safe handling of the strip in the subsequent operation. In addition, sintering also removes undesirable impurities, e.g. surface oxide film and sulphur, from the powder mass provided a suitable atmosphere is used, and this removal may be an additional important aim of sintering. The mechanical properties of the sintered strip, in particular percent elongation, are poor in comparison with fully dense strip, but the sintered strip behaves well during subsequent densification rolling operation. It has been possible to coil the sintered strip on a large radius drum.

The sintering is an important step, and method used for it can control the whole economics of the route. During sintering the green strip must be protected from oxidation, which would not be on the surface but also inside the strip because of connected porosity. Further, any oxide already present on the powder surface must also be reduced. It is therefore, always desirable to use the reducing atmosphere in the sintering furnace. The oxygen and carbon potential of the gas must be in accordance with the requirement. Dry hydrogen and cracked ammonia have been the most common atmospheres used during the sintering for large number of metals.

3 Densification of sintered strip:

The strip obtained after sintering is still relatively porous, although its strength greatly increased in relation to that of the green strip. The densification of the sintered strip can be carried out in two different ways:

3.1 Repeated cold rolling and sintering /annealing cycle

Many workers [18,52,57] have reported that fully dense metal strip can be made from roll compacted and sintered strip by series of cold rolling and sintering/annealing cycles. However, only a few systematic studies have been carried out for understanding of the process. The amount of total cold rolling deformation required for the production of the fully dense strip depends on the porosity in the starting strip. Worn and Perks [16] observed that the initial cold rolling must be limited to about 20% thickness reduction, owing to the presence of highly dispersed porosity which makes the strip crack easily. Hunt and Eborall [15] observed that, in the case of copper, the amount of cold rolling deformation possible between each anneal depends on the density of the strip at the start of each reduction, the variation of the density across the width of the strip, and whether or not strip is to be coiled after rolling. It was reported that the strips are liable to cracking or tearing in a certain density range, i.e. $8 \times 10^3 - 8.4 \times 10^3 \text{ kg m}^{-3}$. The maximum reduction that could safely be applied between anneals in this density range was about 20-25%. It was suggested that below this density range, rolling serves mainly to compact the strip without effecting much extension, and it may be assumed that any longitudinal stress component tending to produce cracking is small. Above this density range the strip is strong enough to withstand the higher stresses involving the extension that takes place.

Sturgeon et al [14] studied the effect of varying amounts of cold rolling on the mechanical properties of the sintered stainless strips. A typical result is shown in figure 2.11 for sintered stainless strip having a density equal to 84% of the theoretical value. It is not mentioned after what amount of cold rolling the strip attained full densification. It maximum after a given level of cold rolling and remains virtually constant as the amount of cold rolling is increased further. The percent elongation, after reaching a maximum value, decreases with further cold rolling. It seems that there is an optimum amount of cold rolling that should be imparted to the sintered strip for the best mechanical properties. Sturgeon speculated that this could result

om changes in the physical dimensions of the testpiece. Such a behaviour could also be caused by fragmentation of inclusions present in the strip.

The greatest disadvantage of this route is that several cold rolling and annealing cycles are required to produce fully dense strip, depending on the initial porosity in the sintered strip. A further disadvantage is encountered when a relatively thick wrought is required. The cold rolling of the sintered strip can be carried out in conventional cold rolling mills. Until the material has attained a density greater than 95% of the theoretical, the speed of rolling must be restricted to avoid crumbling as a result of entrapped air[13].

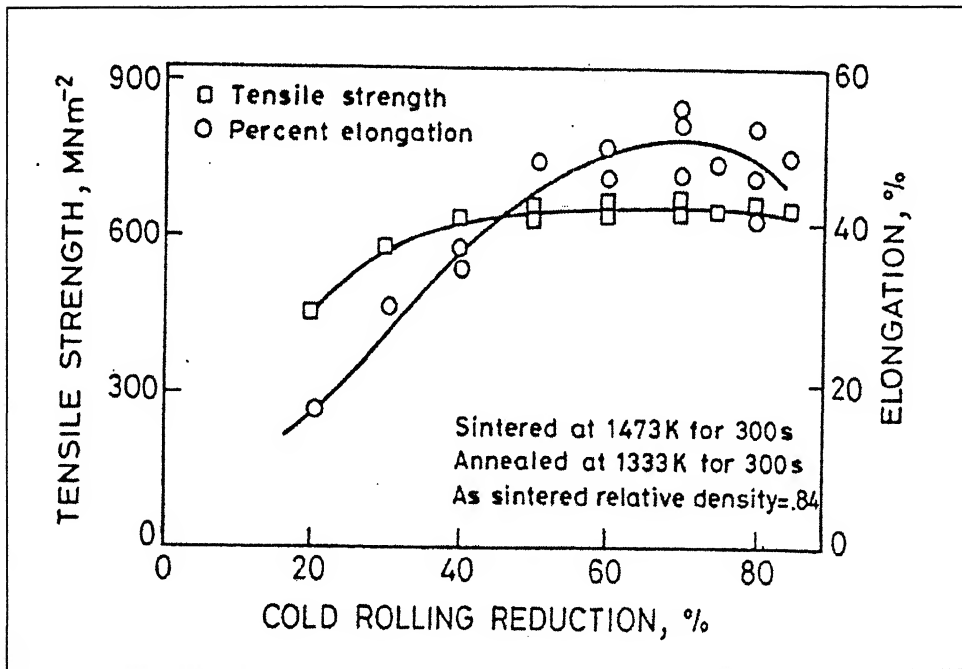


Figure 2.11. Effect of cold rolling reduction on tensile properties (post annealed) of sintered stainless steel strip.

3.2 Hot rolling

Many investigators [12,11,9] have favoured hot rolling after sintering as a means of achieving 100% density in the strip. Metal strips having porosity ranging

from 80 to 25% can be hot rolled to fully density in a single pass. The main advantage of this process is that it is possible to produce a dense strip in one operation; it also reduces the sintering time, and hence the furnace length. Another interesting point is that it is possible to hot roll the sintered strip from the sintering furnace directly to a dense strip, without cooling. As in the previous cases, the amount of thickness deformation actually required by hot rolling to produce a fully dense strip depends on the initial porosity in the sintered strip, and is always greater than that theoretically required. This is because some of the rolling deformation goes in to elongation the strip instead of closing the pores. It has been reported that in practice about twice the theoretical amount of thickness deformation by hot rolling is needed to produce fully dense strip[11].

Whever et al[9] reported that the efficiency of densification E , defined according to the relation

$$E = \frac{\rho_{HR} - \rho}{\rho R} \times 100 \quad (2.2)$$

where R is the percent reduction in thickness, ρ the maximum density attainable, ρ_0 the original perform density, ρ_{HR} the density after hot rolling was greatest for a single large reduction of a low density perform (Figure 2.12). For perform of higher initial density, the maximum efficiencies obtained were much lower than for low density perform.

The change in mechanical properties of the strip as a function of percent thickness reduction by hot rolling has been studied by many workers. For low density starting strip, the mechanical properties remain unaffected initially, but subsequently increased rapidly. However, for high density starting strip, the properties increase from the very beginning. The results of Kimura et al [10] on iron powder showed that the properties of the final finished iron strip obtained from electrolytic iron powder by the PM route involving hot rolling as a means of further densification, compared favourably with those of iron strip obtained from the same powder but made by the PM route involving repeated cold rolling and sintering/annealing cycles as the means

densification. However, in the case of a spong iron powder, they found that the strip made from the former route was slightly inferior to the latter because of its inferior sinterability.

A quantitative relationship between the relative density and the coefficient of compression in hot rolling of porous strip has been derived by Koval'chenko[8] which can be written as follows after rearrangement

$$e_t = 1 - \left[\left(\frac{\rho_0}{\rho} \right)^{\frac{3m+1}{3m}} \left(\frac{1-\rho}{1-\rho_0} \right)^{\frac{1}{3m}} \right] \quad (2.3)$$

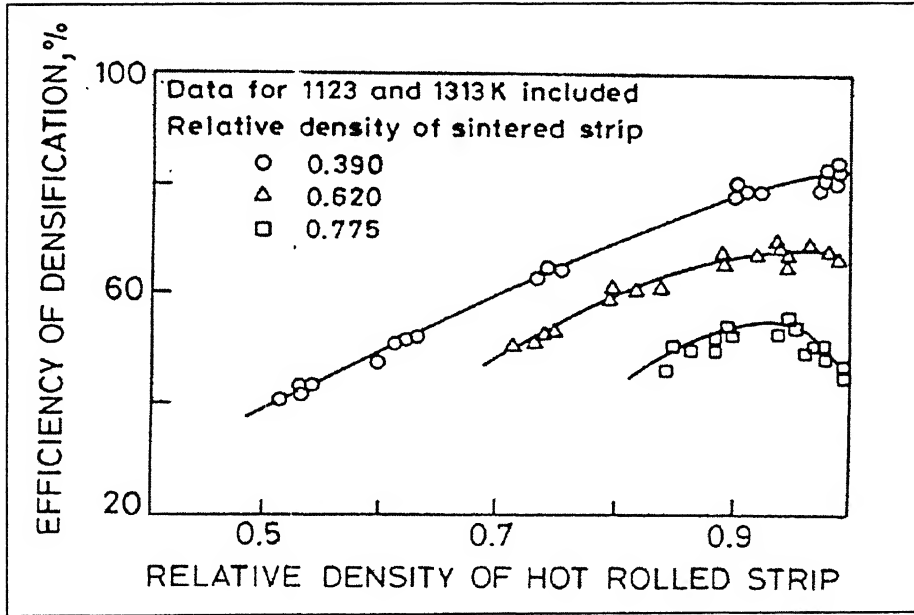


Figure 2.12. Efficiency of densification of sintered steel strip versus final density for single pass hot rolling at different relative density of sintered strip[9]

Where e_t is the fractional thickness deformation given to the strip, m a material constant, and ρ and ρ_0 the relative densities of the strip after and before hot rolling. The above equation can be used to calculate the ratio between the flow in the

itudinal and thickness directions during hot rolling, i.e. apparent plastic
 ision's ratio ν , as follows

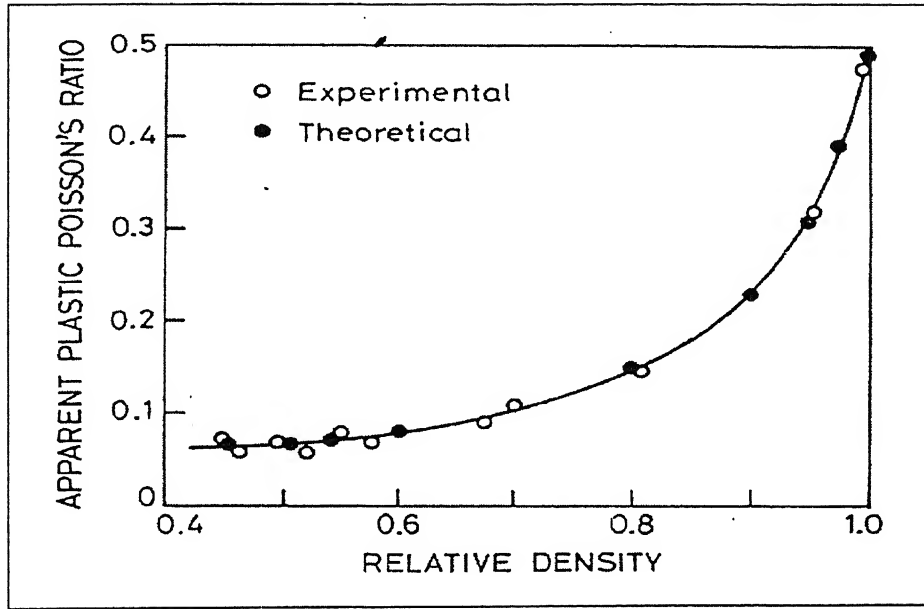


Figure 2.13. Effect of relative density of porous copper strip on apparent plastic
 ison's ratio during hot rolling[7].

$$\frac{1}{2[3m(1-\rho)+1]} \quad (2.4)$$

Bhargava and Dube [7] have found that equation. (2.4) agrees with the
 erimental data obtained by hot rolling a porous copper strip of relative density 0.4
 value of $m=4$, and the results are shown in Figure 2.13.

Final cold rolling and annealing:

Sheet and strip metals are generally cold rolled, followed by suitable anneal
 ore the final finished product is shipped. This is done to achieve optimum
 erties in addition to superior surface finish. Powder metallurgy metal strip
 duced by a hot rolling route would have inferior surface finish, therefore, to pickle
 h strip before cold rolling. In the case of PM strip produced from the repeated cold

ng and sintering/annealing route, this final cold rolling and annealing can be bined with the cold rolling and sintering/annealing carried out for densification oses. The final cold rolling is similar to that used in conventional processing. The l annealing temperature and time for PM strip is generally greater than that used onventional processes, and it has been found to be beneficial in achieving mum properties [6].

It is desirable to start final cold rolling on a fully dense PM metal strip. ever, according to Smucker[5], metal strip within the 96-100% density range ld be cold rolled like a conventional 100% dense metal strip. Therefore, the final l rolling and annealing could also be used for some densification.

Plasticity theory for porous metals

The onset of plastic deformation in porous metals is governed by yield criteria flow rules that are fundamentally different from those for fully dense materials. s is due to the fact that unlike for full-density metals, a significant change in osity is accompanied by volumetric strain in porous metals. A suitable yield erion and stress–strain relationships for porous solids were first proposed by Kuhn . Downey [33] and Green [34]. The theory developed by the above researchers was ended by Shima and Oyane [35] to a general state of stress, leading to a yield erion of the form:

$$\bar{\sigma}_{eq} = [\{ (\sigma_1 - \sigma_2)^2 + (\sigma_2 - \sigma_3)^2 + (\sigma_3 - \sigma_1)^2 \} / 2 + (\sigma_m / f)^2]^{1/2} \quad (2.5)$$

Where σ_m is the hydrostatic stress, f is a material-dependent factor and f' is ratio of the apparent stress applied to the porous solid and the effective stress orted on the metal matrix. From Eq. (2.5), the following stress–strain relations hips i be derived:

$$\dot{\epsilon}_i = \frac{3}{2} \frac{\rho}{f^2} \frac{d\bar{\epsilon}_{eq}}{d\bar{\sigma}_{eq}} \left\{ \sigma_i - \left(1 - \frac{2}{gf^2} \right) \sigma_m \right\} \quad \text{for } i = 1, 2, 3 \quad (2.6)$$

where

$$d\varepsilon_{eq} = \frac{f'}{\rho} \left[\frac{2}{9} ((dv_1 - dv_2)^2 + (dv_2 - dv_3)^2 + (dv_3 - dv_1)^2) + (fd\varepsilon_r)^2 \right]^{1/2} \quad (2.7)$$

and

$$dv_r = dv_1 + dv_2 + dv_3 \quad (2.8)$$

In the above equations, $\bar{\sigma}_{eq}$ and $\bar{\varepsilon}_{eq}$ refer to the equivalent stress and the cumulative equivalent strain, respectively. In cold rolling, due to strain-hardening effects, the deforming material can be characterized by a relationship which provides $\bar{\sigma}_{eq}$ as a function of $\bar{\varepsilon}_{eq}$. The factors f and f' are, in general, functions of the relative density, ρ . For sintered porous metals, Shima and Oyane [35] suggested correlations of the form:

$$f = \frac{1}{A(1-\rho)^B} \quad (2.9)$$

and

$$f' = \rho^C \quad (2.10)$$

where A , B and C are material constants.

2.6 Analysis of the plane-strain cold densification rolling of a sintered porous metal strip by the upper-bound technique[36]

A.R. Deshmukh, T. Sundararajan, R.K. Dube, and S. Bhargava has studied the analysis of the plane-strain cold densification rolling of a sintered porous metal strip by the upper-bound technique. It provides estimates of the total power required for rolling and predicts the variations of velocity, strain components and density within the deformation zone. The roll pressure and the percentage slip at the roll– strip interface are also obtained. Some of the theoretical predictions have been validated by comparison with experimental data obtained from the rolling of porous copper strips.

Influence of rolling parameters

2.1 Friction factor

The effects of the friction factor upon the final strip density, the rolling power then slip are shown in Figure 2.14. For the graphs shown in this figure, the initial relative density of the strip before rolling was taken as 0.7. The exit strip density is observed to increase with the friction factor. This can be attributed to the greater metal flow rate occurring because of better gripping conditions. An examination of slip behaviour also indicates that backward slip is reduced at higher friction factor, causing a greater metal flow rate. The forward slip, on the other hand, is less affected. However, the rolling power increases with the friction factor, because of greater friction work.

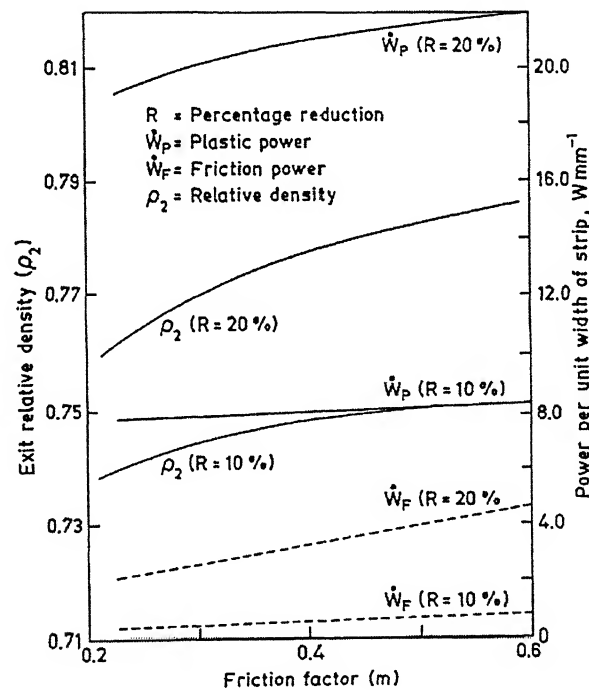


Figure 2.14. Effect of the friction factor on the densification and power.

2.2 Percentage reduction

Figure 2.14 also shows the influence of the percentage reduction upon the densification. For any given friction factor, the exit relative density is greater at higher percentage reduction.

higher reduction. This is explained easily in terms of greater compression as well as the elongation of particles in the rolling direction. The elongation of the particles is an important mechanism of densification for the high value of initial strip density assumed here. Furthermore, it is also observed that the increase in densification is more sensitive to changes in friction factor at greater percentage reduction. This trend can be attributed to the larger arc of contact for greater thickness reduction. As regards the rolling power, both the friction and the plastic deformation components show an increase with percentage reduction. While the friction work increases because of the larger contact area, the plastic work increases due to greater straining of the material. Thus, the total rolling power is also greater for a greater thickness reduction. The backward and forward slips (Figure 2.15) are seen to increase with percentage reduction. In particular, the backward slip becomes very high in magnitude for high thickness reduction for all friction factors.

From Figure 2.16, it is seen that the exit relative density for single-pass rolling increases with the percentage thickness reduction initially but shows a decreasing trend for greater thickness reductions (25% and above). This can be explained in terms of greater backward slip occurring at greater percentage reductions. It was observed that the exponent b decreases rapidly with increase in the slip. This in turn, affects the densification and the exit relative density reduces at greater reduction. Also, greater backward slip causes improper gripping of the strip between the rolls, resulting in less densification. Attempts were made to verify this observation experimentally, however it was noted that the strips developed longitudinal cracks causing splitting of the strip when a thickness reduction of 30% or greater was given in a single pass. Therefore, it was not possible to confirm the above observation.

2.6.1.3 Roll radius

The dependence of the exit density and power components on the roll radius is shown in Figure 2.17. It is evident that the densification behaviour is not influenced significantly by roll radius. This finding supports the conclusion derived from the microscopic view of porous material densification, which indicates that the relative

γ is a function of only the total relative contact area per particle and the axial flow occurring in them. Clearly these microscopic factors are not affected by the distance traveled by the particles in the deformation zone. The exit density, therefore, is fairly insensitive to variation in roll radius. The rolling torque, on the other hand, increases slightly with roll radius. This is contributed partly by friction work and partly by plastic work. The increase in friction work is due to the increase in the arc of contact and that in the plastic work is because of the larger size of the deformation zone. Most of these trends are in conformity with those observed in cold metal rolling [37,38].

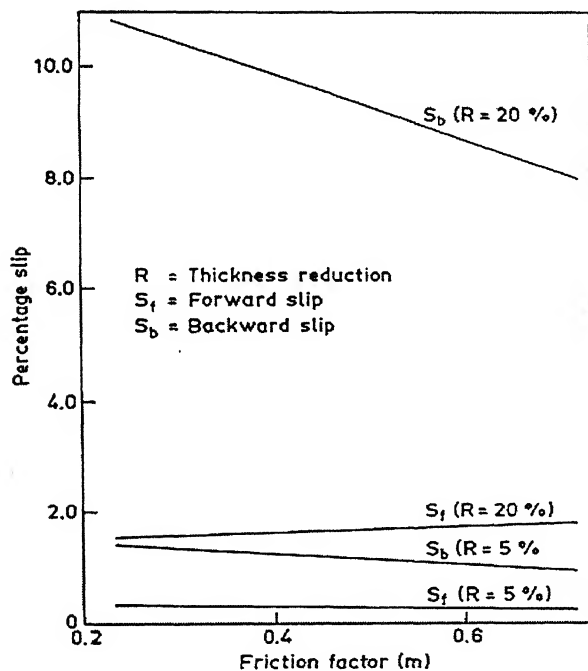


Figure 2.15. Effect of the friction factor on the percentage slip.

4 Roll speed

It can be seen from Figure 2.18 that the densification is unaffected by the roll speed, while the power increases linearly with the roll speed. The insensitivity of the densification to the roll speed is again related to the microscopic features of porous rolling discussed in the previous section. The roll speed influences only the

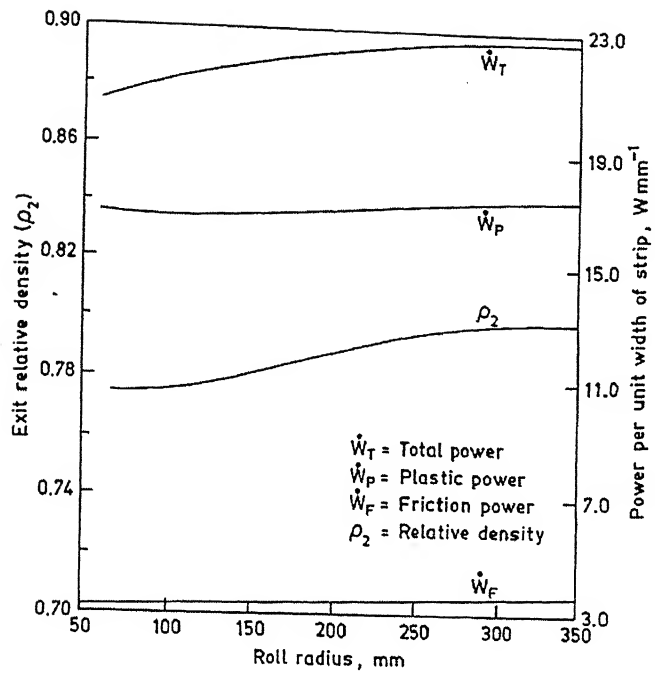


Figure 2.16. Effect of the thickness reduction on the densification.

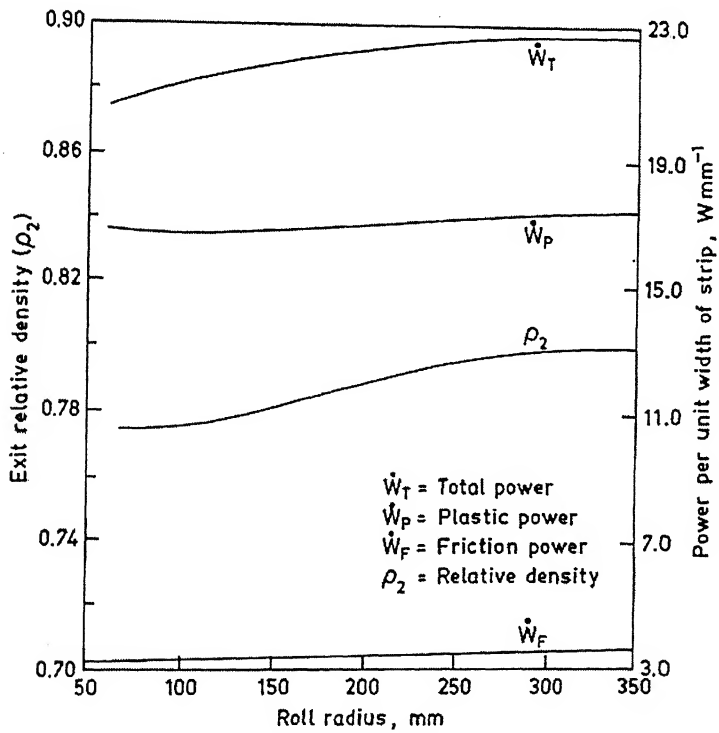


Figure 2.17. Effect of the roll radius on the densification and the power.

Travel time of a particle through the roll gap and does not affect the inter-particle contact area for longitudinal flow in them. However, a greater roll speed results in greater strain rates, which in turn, lead to greater work of deformation. It was found that the backward slip also tends to increase with the roll speed, thereby causing greater frictional dissipation. Of these two contributions, the change in plastic deformation power is greater compared to that of the friction power.

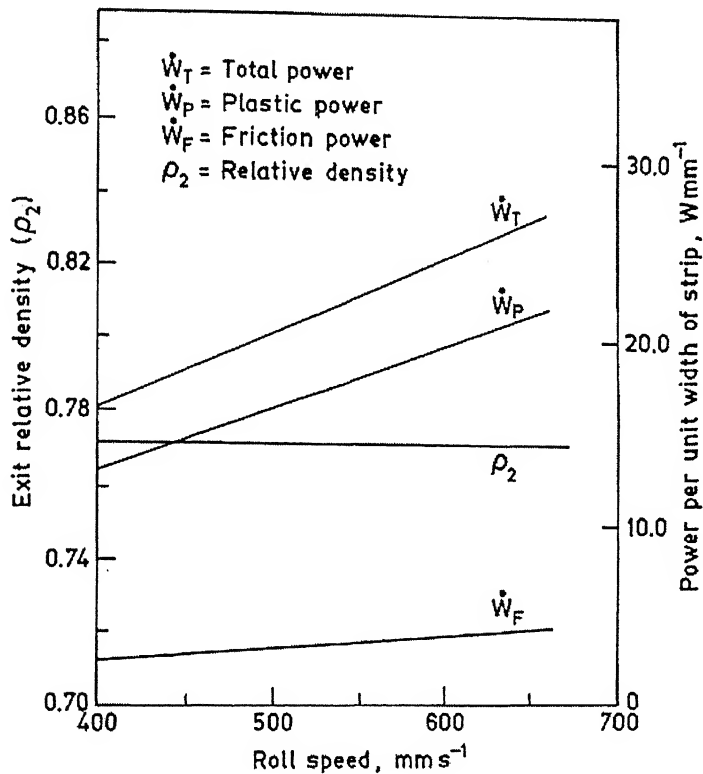


Figure 2.18. Effect of the roll speed on the densification and the power.

2.6.1.5 Initial relative density of the strip

The incremental change in relative density, $\Delta\rho$, from the entrance to the exit as a function of the initial relative density, ρ_1 , is shown in Figure 2.19. It is observed that the percentage increase in relative density decreases for greater initial relative density, because of the larger area of contact between neighboring particles and the smaller available void space surrounding them. Due to these two factors, the resistance offered by the material for further deformation

increases, resulting in a greater value of yield stress. Therefore, the rolling power per unit width also increases with the initial relative density. Clearly, the greater yield stress value increases the plastic work contribution. The frictional work also increases, because of the larger actual contact area between the rolls and the porous strip and also because of the greater yield stress value.

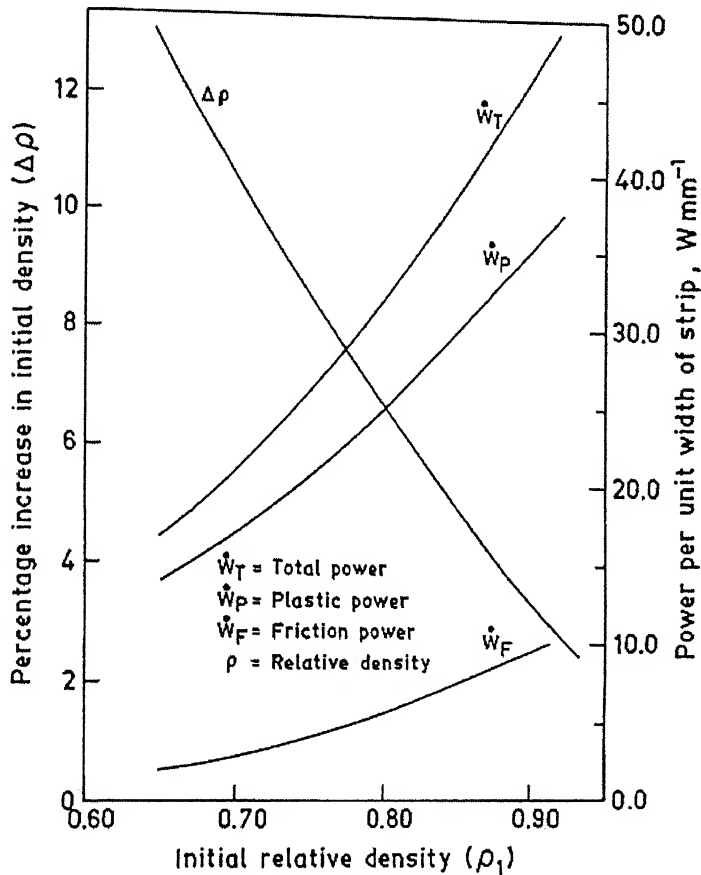


Figure 2.19. Effect of the initial strip thickness on the densification and the power.

2.7 Object of the present work

An understanding regarding the densification of porous metal performs, as a function of rolling thickness reduction have been studied by following methods:

- 1) Generating the experimental data and fitting with an empirical relationship.

- 2) Analysis by solving constitutive equations written for the plane-strain conditions that exist during rolling of a flat sheet.
- 3) Efforts have also been made to generate such an understanding by analyzing densification of porous material using the finite element method (FEM) approach.

A micro-level description of densification rolling of a porous metal strip, however, requires an understanding of the changes that take place in

- (i) The free surface area of particles.
- (ii) The average coordination number and the average contact area per particle.
- (iii) Average pore size and aspect ratio and pore size distribution.
- (iv) Aspect ratio of grains.
- (v) Shape of pores.

Empirical approach as well as the approach based on stress-strain analysis, though giving satisfactory engineering solutions, fail to generate the basic micro-level fundamental mechanisms of pore removal and changes that occur in other micro-level structural parameters of the porous metal strip during densification rolling. Stereology is a collection of mathematical methods that relate the parameters defining a spatial structure to lower dimensional measurements made on sections through the structure. Variation in the parameters such as grain size distribution, pore size distribution, surface area per unit volume of pores, mean grain size, contiguity and aspect ratio of pores/particles which can be conveniently measured by stereological analysis. Very limited observations regarding densification rolling of a porous metal strip using stereological analysis have, however, been reported in the literature.

The present study was undertaken to fill this gap. Porous nickel strips were prepared and were subsequently subjected to cold densification rolling for different thickness reductions. Results obtained through stereological observations have been described.

In our study Ni powder is being compacted by die compaction, then sintered and finally subjected to different amount of deformation by means of cold rolling maintaining plain strain condition.

CHAPTER 3

EXPERIMENTAL PROCEDURE

The Present chapter deals with various experimental techniques used to both process and characterization of Cold Rolled Ni strip.

3.1 Raw material

3.1.1 Elemental nickel powder

Extra pure, Argon packed Ni – powder of particle size between 74 micron to 104 micron, supplied by SISCO Research Laboratory Pvt. Ltd. Bombay. Maximum limit of impurity present in the powder are 0.005 % in the form of Cobalt and 0.1 % in the form of Iron.

3.2 Compaction

The Powders were compacted in hydraulic press by applying pressure 150 kg/cm² for 10 seconds using Methylcellulose as a binder. The compacts were pressed in rectangle pellet form with length of 200mm, width of 150 mm and height of 3.95 mm. To facilitate pressing, zinc-stearate was used as die-wall lubricant. The die was made of high chromium high carbon steel was cleaned with acetone prior fill. Lubrication facilities compaction and subsequent removal of green compacted samples.

3.3 Sintering

The Green strips were sintered in the same one-end muffle type furnace. Sintering was done in inert gas atmosphere. Argon was used for this purpose. After sintering the strips were slowly transferred to the cooling zone of the furnace where they were cooled in inert gas atmosphere in order to avoid oxidation of the sintered sample and transferred quickly to the desecrator. Sintering was carried out for 90 minutes. Sintering temperature was maintained at 1073K. The main purpose of sintering is to provide adequate strength to the material for cold rolling in the

subsequent step. The temperature and time of sintering does not provide sufficient densification of material.

3.4 Cold Rolling of Sintered Pellet

The sintered product is further cold rolled with different amount of thickness reduction starting from one end to other along the length. The varying amount of thickness reduction is 0% to 70 % in the present case of study. Cold rolling of sintered strip was done on a single strand, non-reversing type two-high rolling mill, having 135 mm diameter rolls, rotating at a fixed speed of 55 r.p.m.

3.5 Quantitative Metallography

3.5.1 Specimen Preparation

The cold Rolled strip was sectioned longitudinally to get flat surface. For better microstructural observations a mixture of epoxy resin and hardener under vacuum fills the pores in the strip. This was followed by cold mounting. Care was taken while mounting in order to maintain good gripping of samples with in the mount and flatness of sample. Cold rolled strip was polished manually on a 'Lunn major Polisher of Struers make, Denmark' having four grades of emery papers 1/0, 2/0, 3/0 and 4/0 in that order, followed by fine wheel polishing with suspended 0.03 μm size alumina in distilled water.

3.5.2 Microstructural Studies

Ni and its alloys give good contrast in micrograph etching with Merica's reagent (50cc, 70 %Nitric acid + 50cc, 50% acetic acid). All the optical micrographs were taken in etched condition by LEICA@500IW image analyzer. Some micrographs were taken in unetched condition for better analysis of the microstructure. The volume fraction of pores, average pore size, aspect ratio of pores, pore size distribution, surface area of pores per unit volume, aspect ratio of grains, contiguity of solid-solid contact were characterized manually through microstructural analysis with the help of LEICA@500IW image analyzer.

3.5.2.1 Volume fraction of Pores

In quantitative metallography, systematic point count analysis was carried out to evaluate the volume fraction of pores of as-received sample by cold rolling of sintered Ni strip followed by filling the pores in the strip by the mixture of epoxy resin and hardener under vacuum condition. In systematic point count analysis, a square grid with 30 grid points was superimposed on the microstructure. The number of grid points falling on the pores were counted systemically and compared with total number of grid points. If total number of grid points falling on the phase of interest is P_i and total number of grid points is P_a then the point fraction is given by-

$$P_p = \frac{P_i}{P_a} \quad (3.1)$$

It will give the volume fraction (V_v) of the pores. The advantage of using the systematic point count analysis is that the relative error is low (10%) as compared to other methods available. The same procedure was carried out on 8 fields of views of same cold rolling reduction, and mean was considered as final result.

From appendix A Hilliard and Cahn [39] have concluded that the best method for volume fraction analysis is a systematic point count in which a grid is superimposed on a sequence of areas selected either randomly or systematically from the plane of polish. The total fraction of grid corners falling on a particular phase provides a unbiased estimate of the volume fraction of that phase.

3.5.2.2 Average Pore size

The pore size was calculated from volume fraction of pores (V_v) and surface area per unit volume (S_v) of pores. The average pore size is related to V_v and S_v discussed below-

$$\bar{l} = \frac{\sum l_i}{n} = \frac{\sum l_i}{L} \frac{L}{n} = L_L \frac{2}{P_L}$$

$$= V_v \frac{2}{P_L} \quad (\text{From } V_v = L_L = P_p)$$

$$\bar{l} = P_p \frac{2}{P_L} \quad (3.2)$$

$$= V_v \frac{4}{S_v} \quad (\text{From } P_L = \frac{S_v}{2})$$

where,

\bar{l} = average pore size

n = number of intersection on solid-pore interface

S_v = Surface area of pores per unit volume

V_v = Volume fraction of pores

3.5.2.3 Aspect ratio of Pores

Aspect ratio of pores was calculated by manual measurement of length and width of 20 pores on a particular cold rolling reduction by using length measurement tool by using image analysis software. The mean was considered as final aspect ratio.

3.5.2.4 Surface Area per unit Volume of pores(S_v)

Surface area per unit volume of the pores was calculated using 10 lines of equal length. The total number of points of intersections with the solid-pore contact was calculated for 8 fields of view for the same cold rolling reduction. Finally, this produced the points per unit length (P_L). Then (S_v) was calculated as

$$S_v = 2 P_L \quad (3.3)$$

where, L = Length of line in terms of μm varies depending upon the magnification.

3.5.2.5 Contiguity of Solid-Solid contact

Contiguity is a measure of solid-solid contact in the cold rolled Ni metal strip, and it is given mathematically as

$$C_g = \frac{2P_L^{S/S}}{2P_L^{S/S} + P_L^{S/P}} \quad (3.4)$$

where,

C_g = Contiguity of the solid-solid contacts

$P_L^{S/S}$ = Number of intercepts made by solid-solid contact per unit length of test line.

$P_L^{S/P}$ = Number of intercepts made by solid-pore contact per unit length of test line.

Contiguity would vary between 0 and 1. A value 0 indicates that there is no solid contact and a value of 1 implies 100% contiguous structure or we can say structure without any pores. The same calculation was done on 8 fields of view at a particular cold rolling reduction. The mean value was taken as contiguity factor of that sample.

3.5.2.6 Aspect ratio of grains

Aspect ratio of grains was calculated by manual measurement of length and width of 20 grains on a particular cold rolling reduction by using length measurement tool in image analysis software. The mean was considered as final aspect ratio.

Scanning Electron Microscopy

The Fracture surface of the cold rolled metal strips at 0%, 40%, 45%, 55% cold rolling reductions were analyzed under a FEI, Quanta-200 HV Scanning Electron Microscope (SEM).

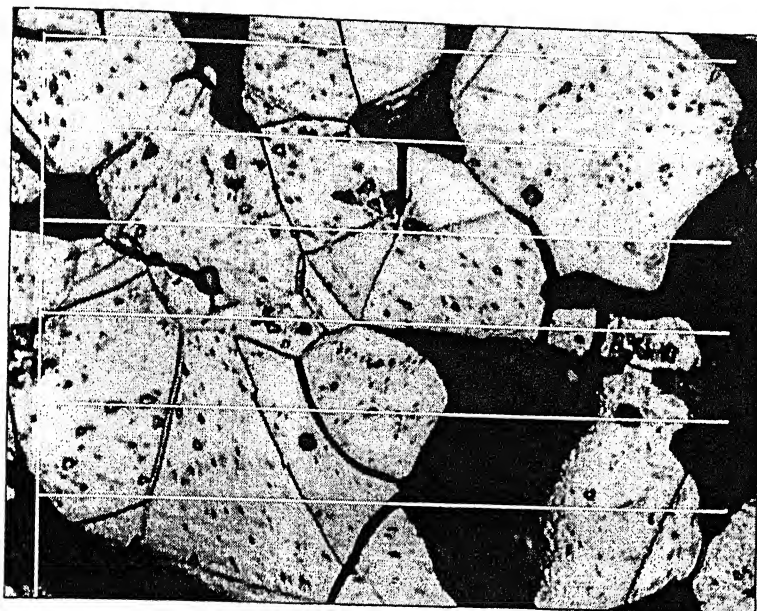


Figure 3.1. Superimposing grid on a Micrograph for calculation of Contiguity ratio.

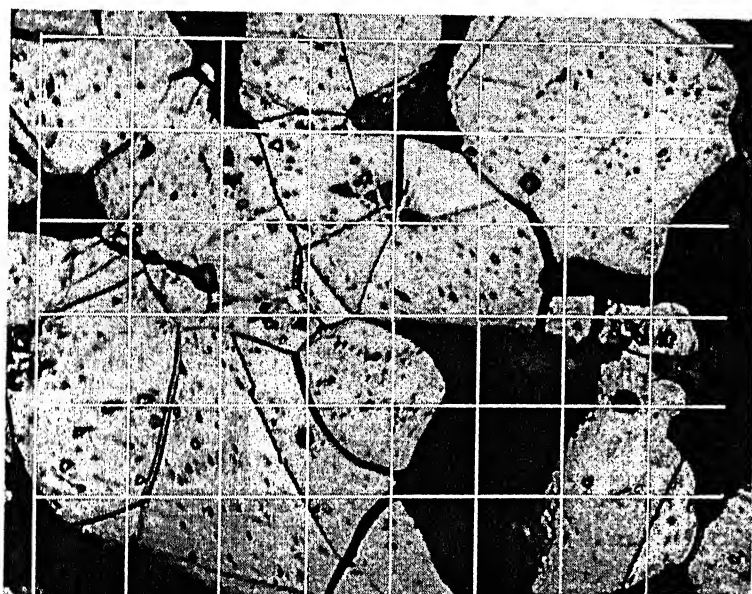


Figure 3.2. Superimposing grid on a Micrograph for calculation of volume fraction of particular phase.

CHAPTER 4

EXPERIMENTAL RESULTS

The experimental results of the present investigation are described in this chapter.

4.1 Starting material

Compacted and Than Sintered product from Ni powder was the starting material for the cold rolling deformation. 0 % cold rolling reduction shows the starting material. At this stage optical micrograph and SEM picture shown in Fig 1 and Fig 2 respectively. At 0 % cold rolling reduction following metallographic quantities were observed.

Volume Fraction of pores	0.309
Surface area of pores per unit volume	$0.043 \frac{\mu m^2}{\mu m^3}$
Contiguity ratio of solid-solid contact	0.207
Aspect ratio of pores	3.80
Average pore size	$28.751 \mu m$
Aspect ratio of grains	1.1

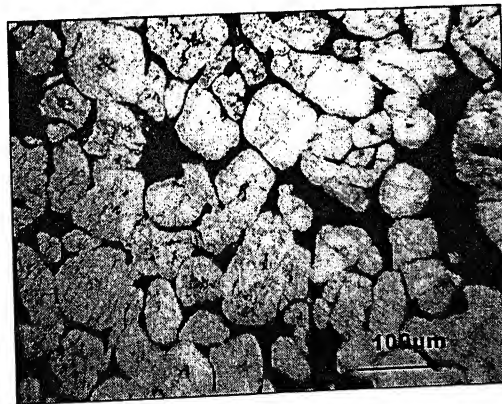


Figure 4.1 Optical Micrograph at 0% cold rolling reduction

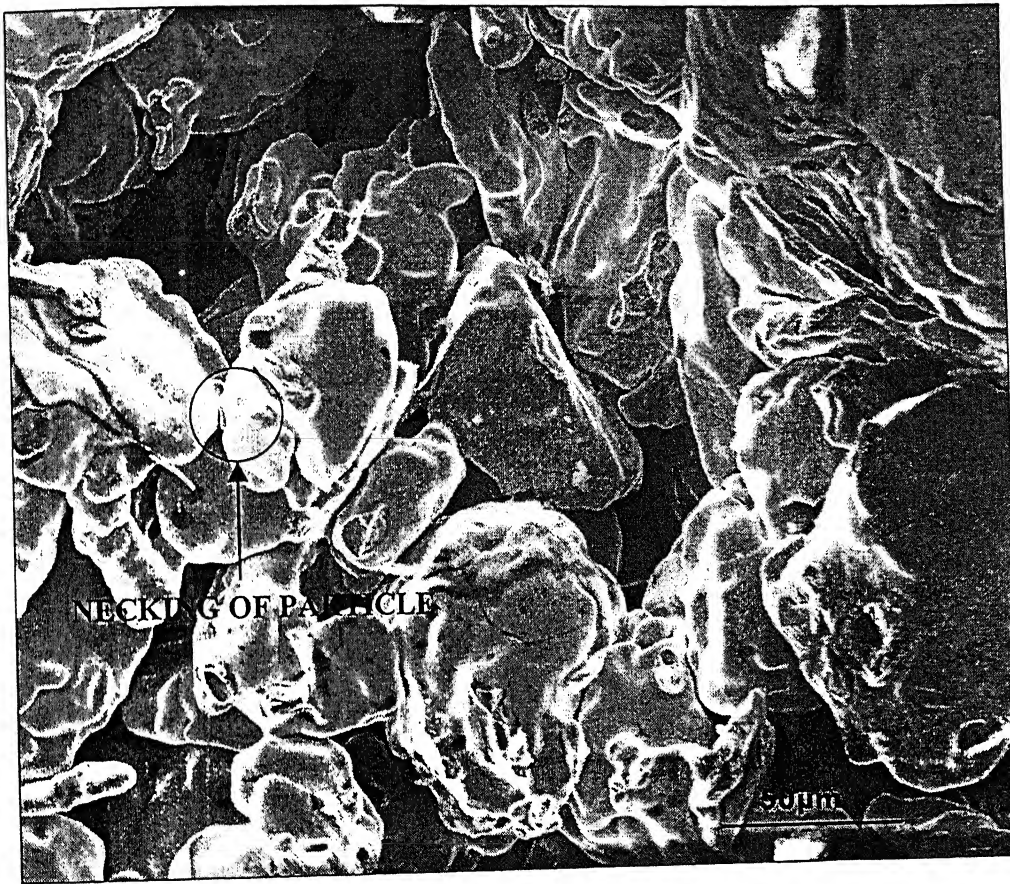
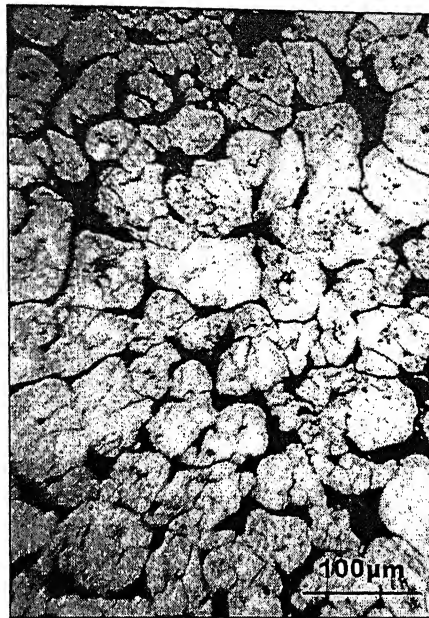
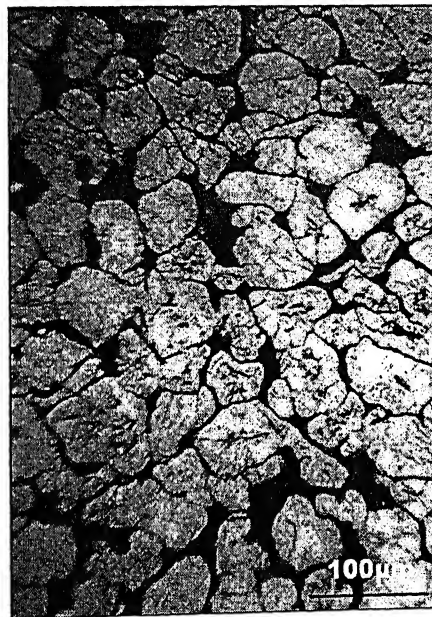


Figure 4.2. SEM of the fracture surface of the metal strip at 0% cold rolling reduction



→
Rolling Direction

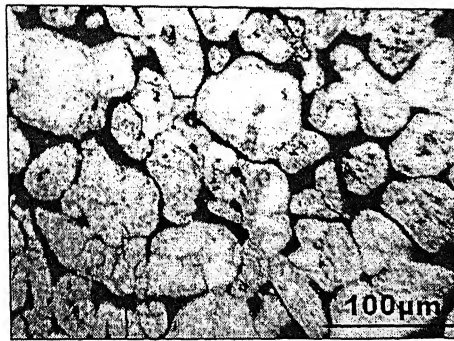
(a)



→
Rolling Direction

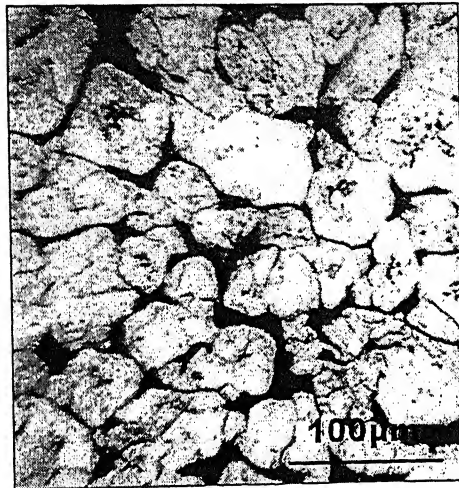
(b)

Figure 4.3. Optical Micrographs of the metal strip at (a) 20% and (b) 25% cold rolling reductions.



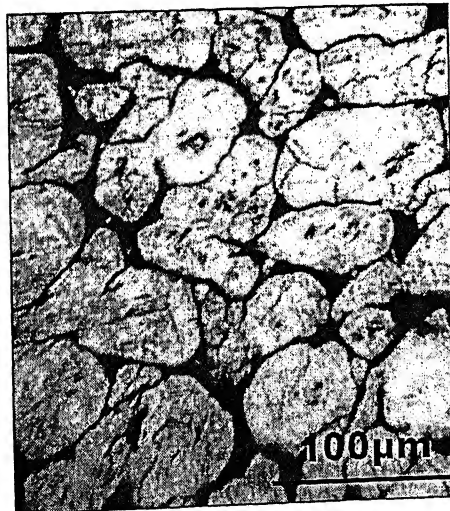
→
Rolling Direction

(a)



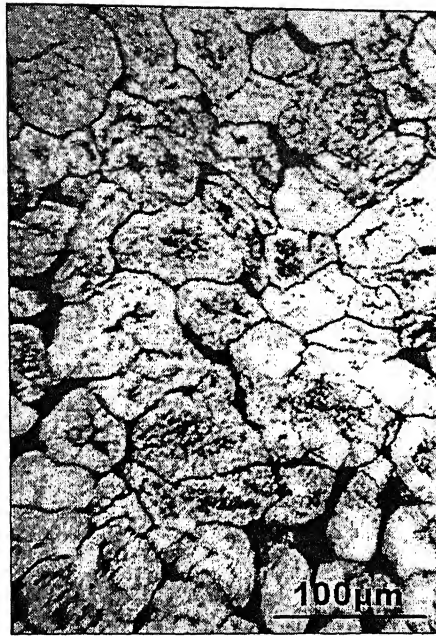
→
Rolling Direction

(b)



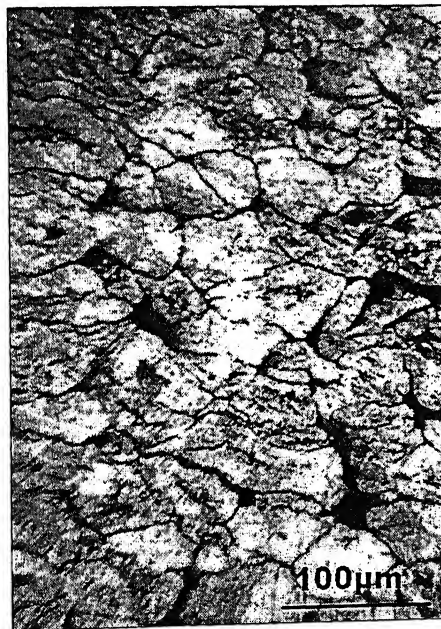
→
Rolling Direction

(c)



→
Rolling Direction

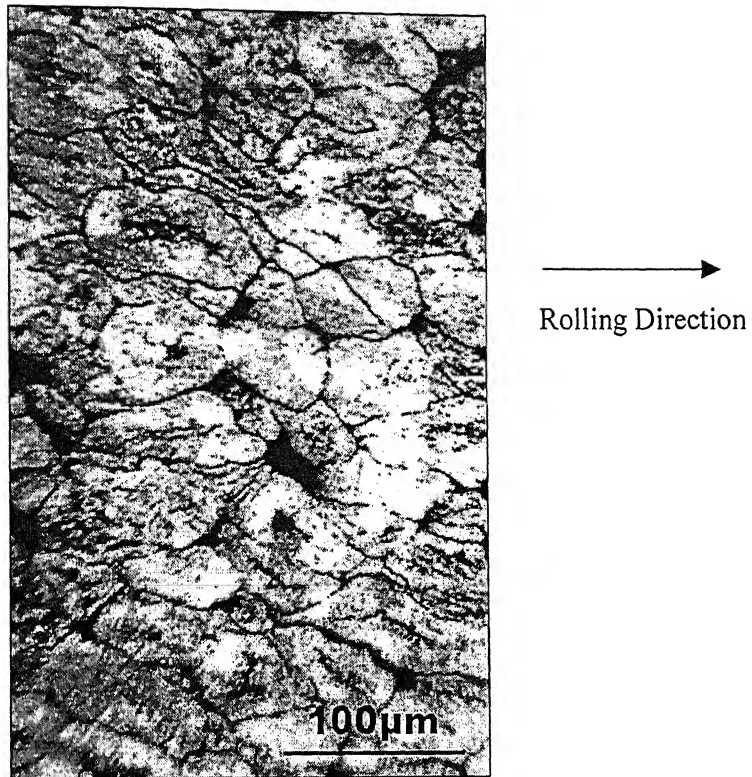
(d)



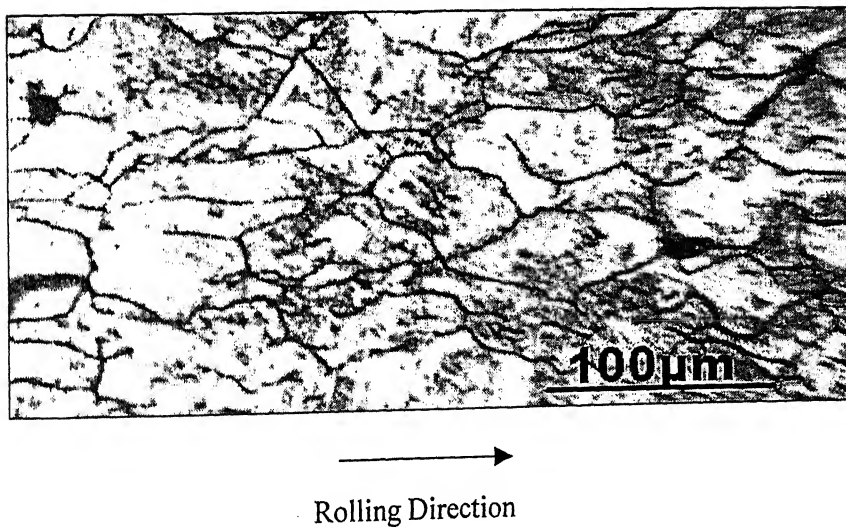
→
Rolling Direction

(e)

Figure 4.4. Optical Micrographs of the metal strip at (a) 30%, (b) 35%, (c) 40%, (d) 45% and (e) 50% cold rolling reductions.



(a)



(b)

Figure 4.5. Optical Micrographs of the metal strip at (a) 55% and (b) 60% cold rolling reductions

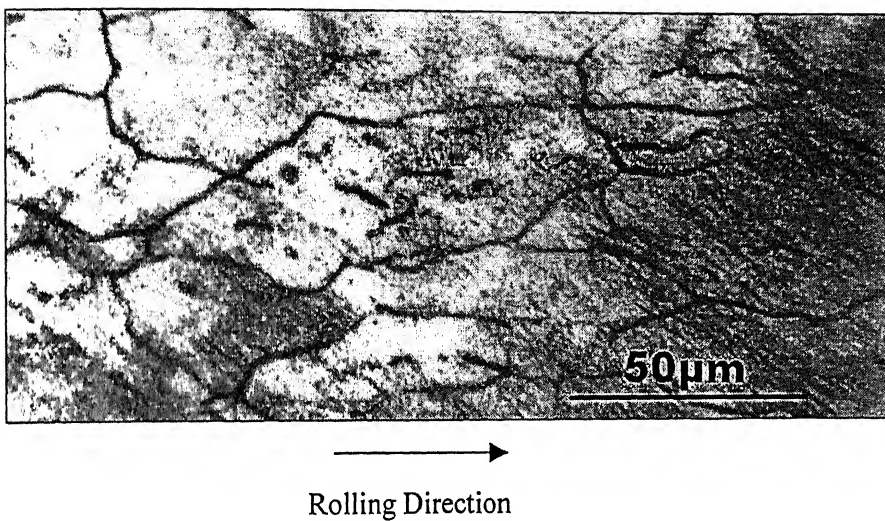
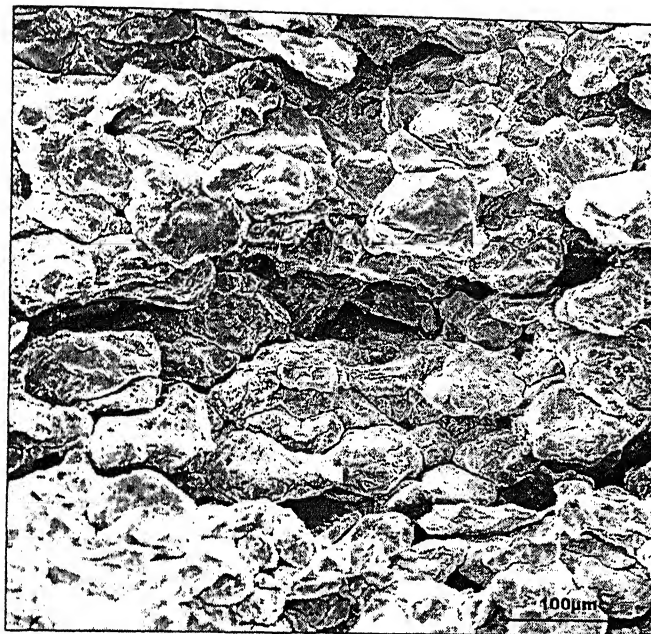


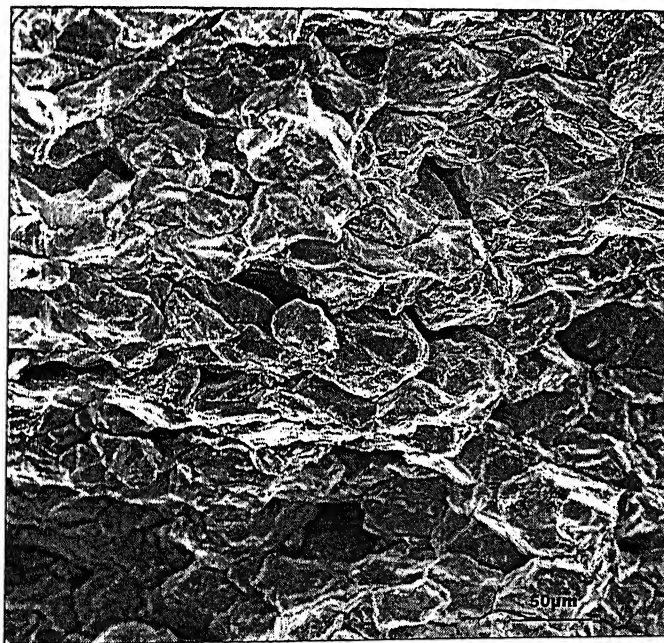
Figure 4.6. Optical Micrograph of the metal strip at 65% cold rolling reduction.

गुरुप्राप्तम काशीनाथ केलकर पुस्तकालय
 भारतीय प्रौद्योगिकी संस्थान कानपुर
 अवाप्ति क्र० A...149295...



→
Rolling Direction

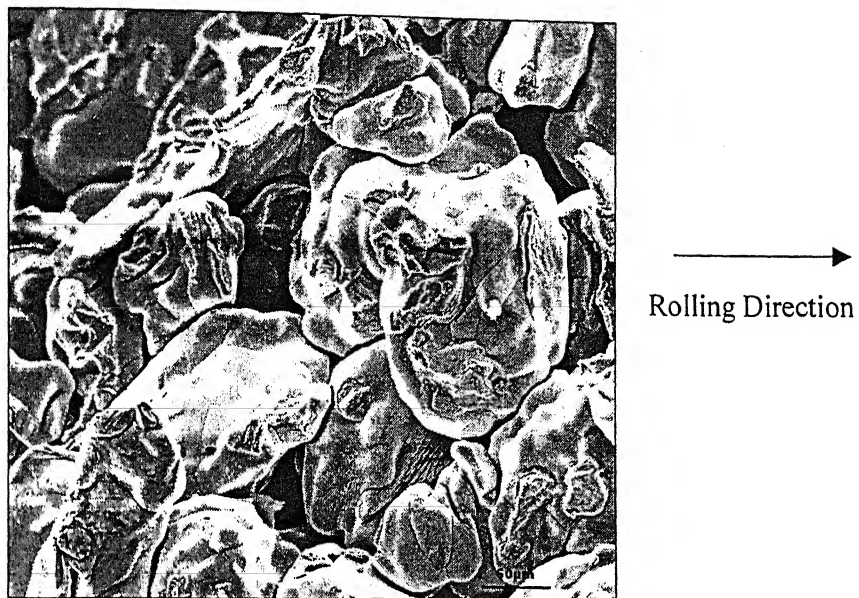
(a)



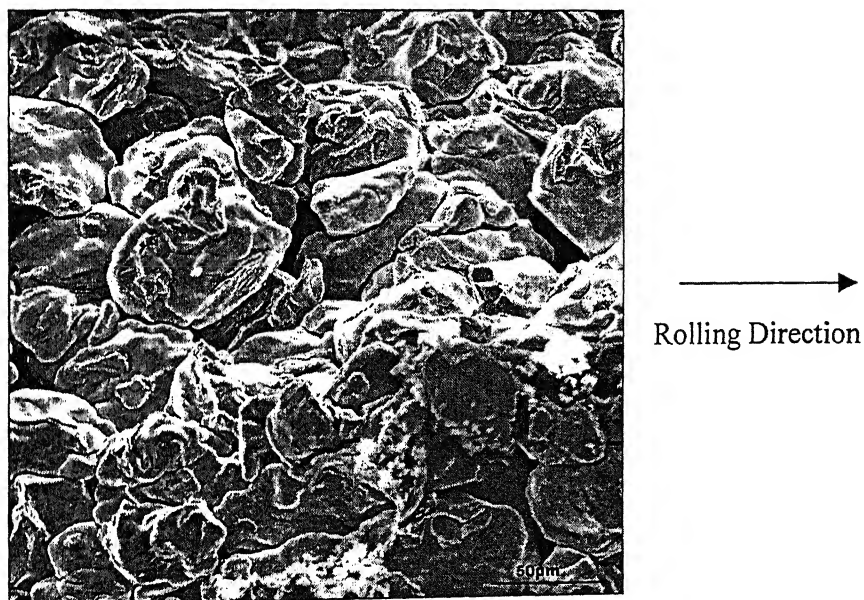
→
Rolling Direction

(b)

Figure 4.7 SEM of the fracture surface of the metal strip at 40% cold rolling reduction

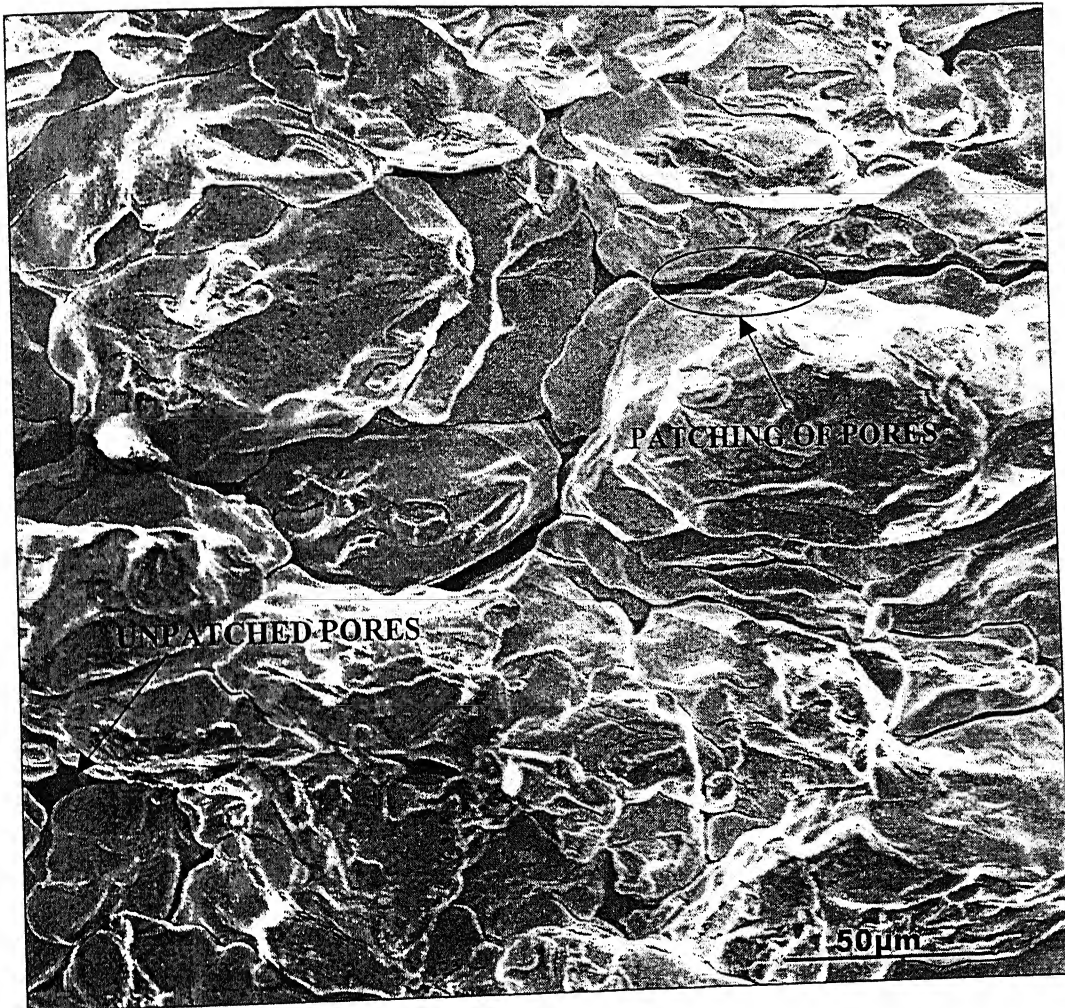


(a)



(b)

Figure 4.8 SEM of the fracture surface of the metal strip at 45% cold rolling reduction



→
Rolling Direction

Figure 4.9. SEM of the fracture surface of the strip at 55% cold rolling reduction

4.2 Densification behavior

Densification behavior can be explained with the help of following observations.

4.2.1 Effect of cold rolling reduction on volume fraction of pores

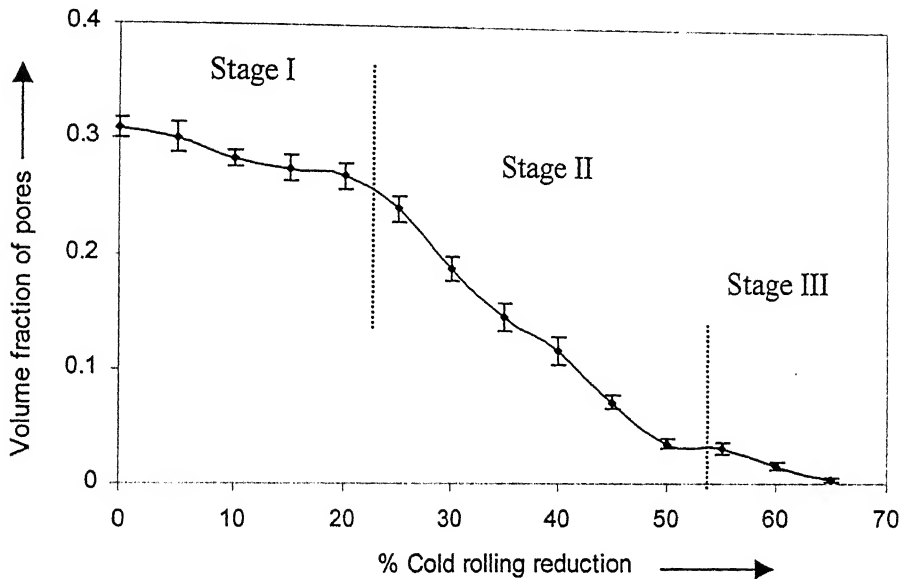


Figure 4.10. Effect of cold rolling reductions on volume fraction of pores. Error bar is representing the 95 % CL(see Appendix B)

Volume fraction of pores continuously decreases with increase in %cold rolling reduction as shown in Figure 4.10. Initial Volume fraction (At 0% cold rolling reduction) is 0.31. At the initial stage up to 25% cold rolling reduction, slow decrease in volume fraction of pores was observed, due to elongation of pores and very less patching of pores. At this stage only big pores are fragmented in to small pores. Volume Fraction of pores decreases at higher rate between 25% cold rolling reductions to 50 % cold rolling reduction, due to sufficient amount of patching of pores in this range. At 50 % cold rolling reduction 3 % pores were observed. After

around 50 % cold rolling reduction again slow decrease in volume fraction of pores with increase in cold rolling reduction was observed, due to greater cold rolling stress was required for patching of minute pores. At 65 % cold rolling reduction almost all the pores are patched up and Ni metal strip without pores was obtained.

4.2.2 Effect of cold rolling reduction on surface area of pores per unit volume

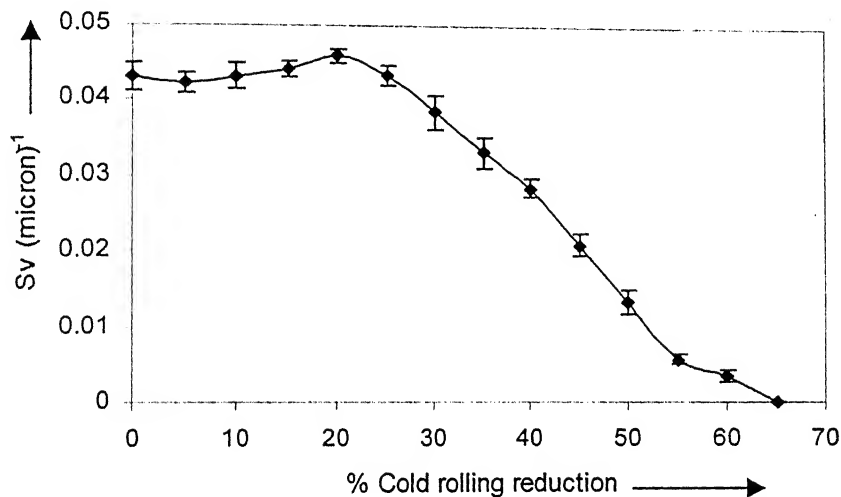


Figure 4.11. Effect of cold rolling reductions on Surface area of pores per unit volume. Error bar is representing the 95 % CL.

At the initial stage up to 15 % cold rolling reduction there was no change in surface area per unit volume of pores as shown in Figure 4.11. At 20 % cold rolling reduction small increase in surface area per unit volume of pores was observed due to elongation of pores. Then after 23 % cold rolling reduction continuous decrease in surface area per unit volume of pores was observed. At the later stage after 50% cold rolling reduction decrease in surface area of pores per unit volume with increase in % cold rolling reduction slows down, because we have to apply greater stress for patching of minute pores.

4.2.3 Effect of cold rolling reduction on contiguity of solid-solid contact

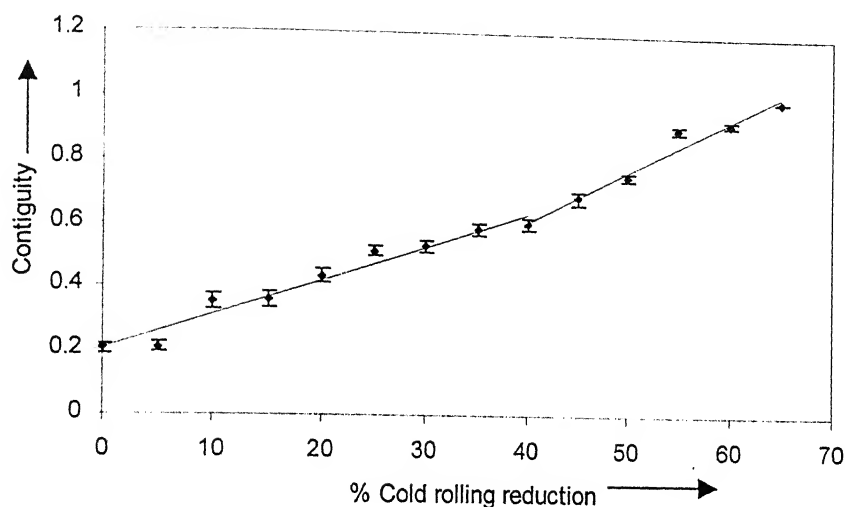


Figure 4.12. Effect of Cold Rolling reduction on Contiguity of solid-solid Contact.

Contiguity is a measure of solid-solid contact in the cold rolled Ni metal strip, and it is given mathematically by equation 3.4. Contiguity would vary between 0 and 1. A value 0 indicates that there is no solid contact and a value of 1 implies 100% contiguous structure or we can say structure without any pores. No change in Contiguity of solid-solid contact was observed till 5 % cold rolling reduction as shown in Figure 4.12. After that Contiguity increase with increase in cold rolling reduction due to fragmentation and patching of pores. Slope of the two straight lines in Figure 4.12 shows the rate of change of contiguity with the change in % cold rolling reduction.

4.3 Morphology of Pores

4.3.1 Effect of cold rolling reduction on aspect ratio of pores

Initially up to around 15% Cold rolling reduction Aspect ratio of pores gradually increase with increase in cold rolling reduction as shown in Figure 4.13, due to very small amount of elongation of pores. After 15 % cold rolling reduction aspect ratio of pores decrease due to fragmentation of pores and after 35% cold

rolling reduction there is an increase in aspect ratio because of elongation of the fragmented pores. After 40% cold rolling reduction aspect ratio of pores decrease with increase in % cold rolling reduction due to fragmentation of the elongated pores. And finally very small pores of aspect ratio of 1 at round 60% cold rolling reduction were observed.

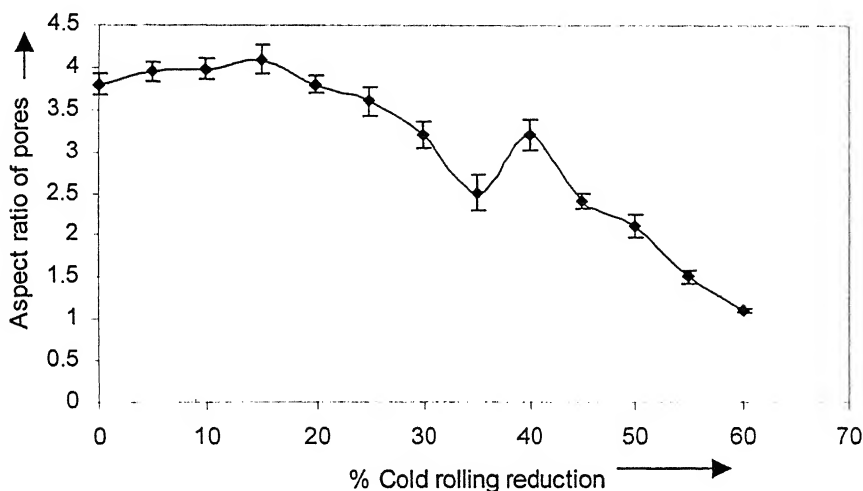


Figure 4.13. Effect of Cold Rolling reduction on Aspect Ratio of Pores.

4.3.2 Effect of % cold rolling reduction on average pore size

Average size of pores continuously decreases with increase in cold rolling reduction as shown in Figure 4.14. Initial (at 0% cold rolling reduction) average pore size is 29 micron. Up to 5 % cold rolling reduction no change was observed in average pore size. Average pore size decrease with the increase in % cold rolling reduction because of fragmentation of big pores in to smaller pores and patching of pores. Patching of big pores is easier than that of the smaller pores.

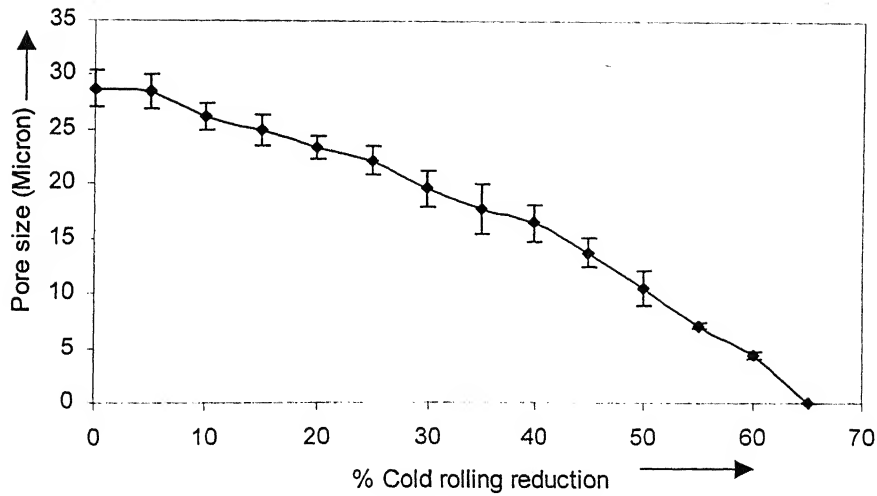


Figure 4.14. Effect of cold rolling reduction on the average pore size. Error bar is representing the 95 % CL.

4.3.3 Effect of cold rolling reduction on aspect ratio of grains

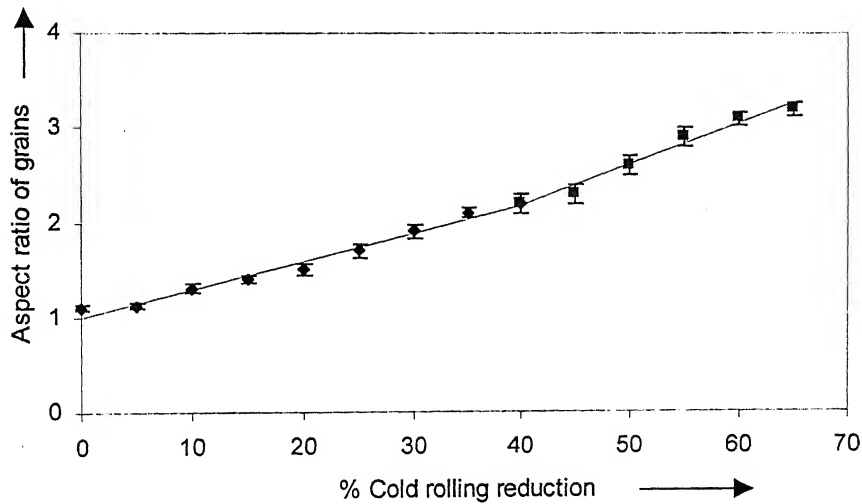
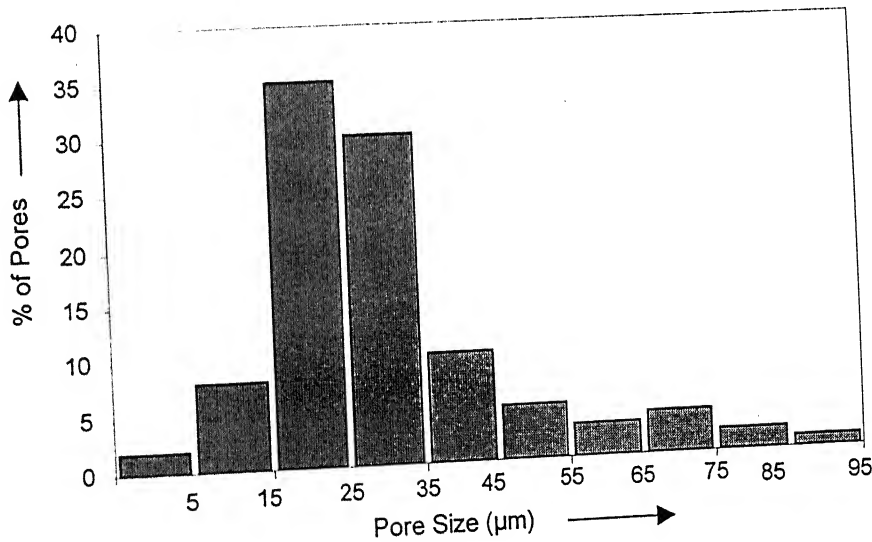


Figure 4.15. Effect of Cold Rolling reduction on Aspect Ratio of Grains.

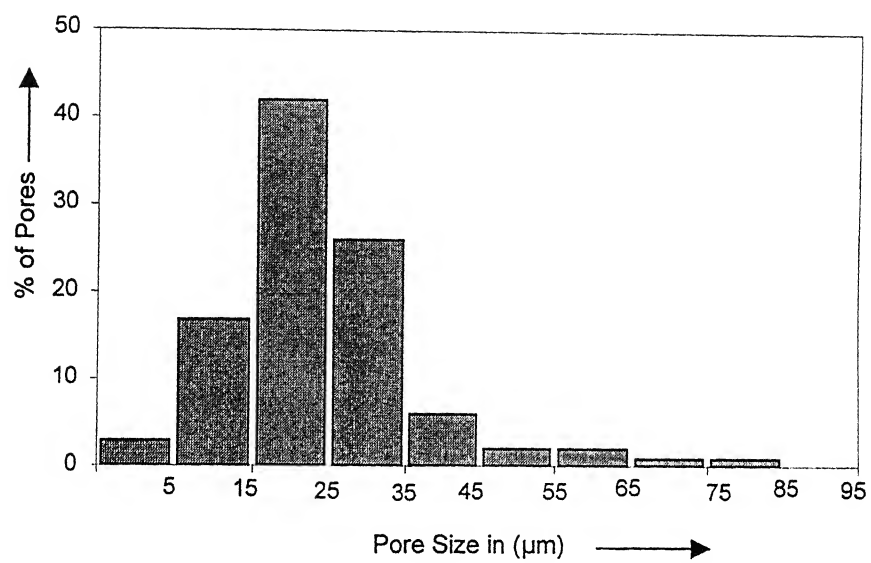
Aspect ratio of grains continuously increases with increase in % cold rolling reduction according to Figure 4.15. Aspect ratio of grains is 1.1 at 0% cold rolling

reduction and increases to 3.2 at 65% cold rolling reduction due to elongation of grains due to rolling pressure. At the initial stage slow change in aspect ratio of pores was observed because of larger volume fraction of pores. At the later stage after 50 % cold rolling reduction fast increase in aspect ratio was observed because of very less volume fraction of pores. At later stage, the cause of rapid change in aspect ratio of grains is that large part of the rolling pressure is used in elongation of the grains. Slope of the two straight lines in Figure 4.15 shows the rate of change of aspect ratio of grains with the change in % cold rolling reduction

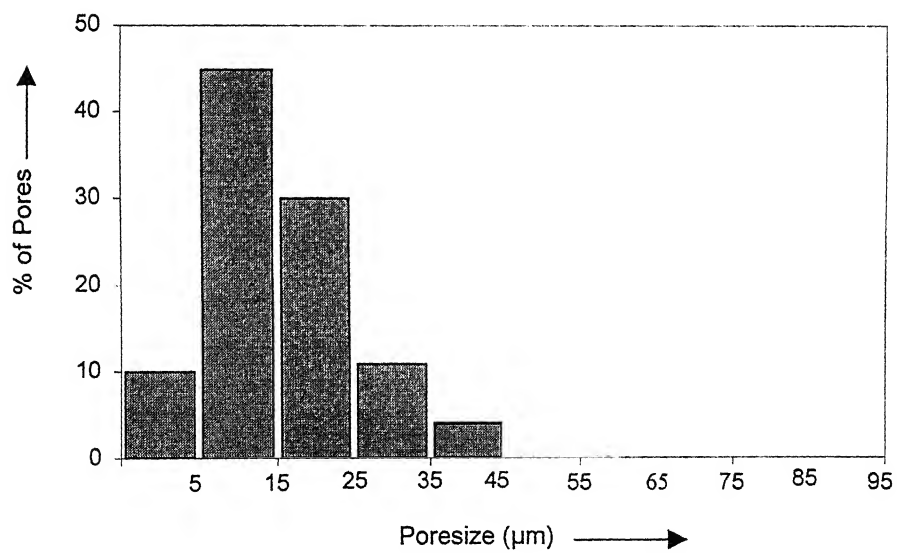
4.3.4 Effect of cold rolling reduction on pore size distribution



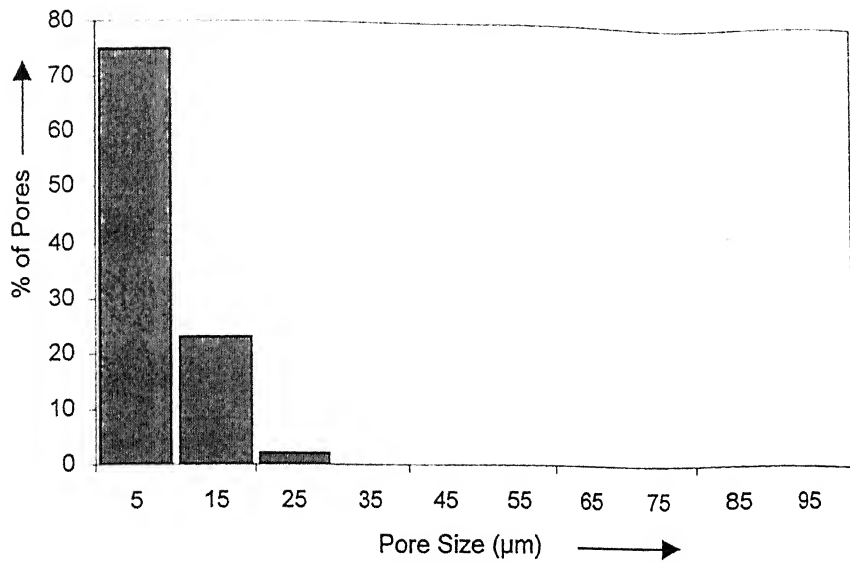
(a)



(b)

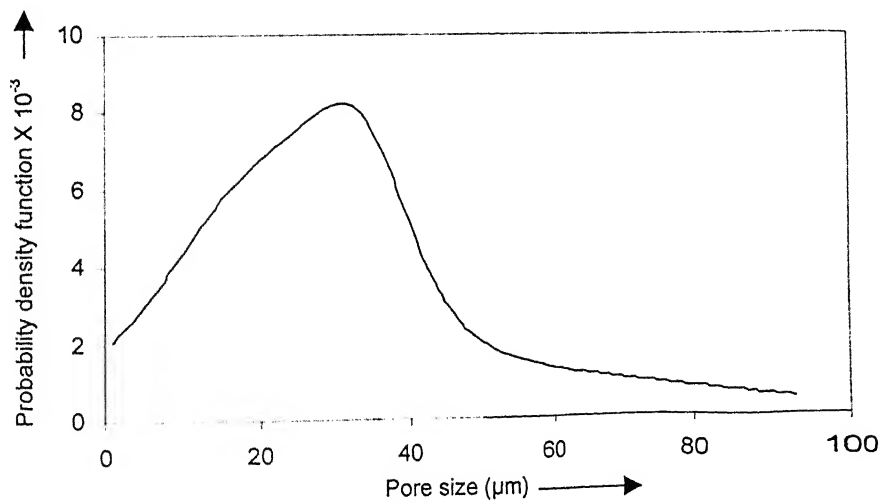


(c)

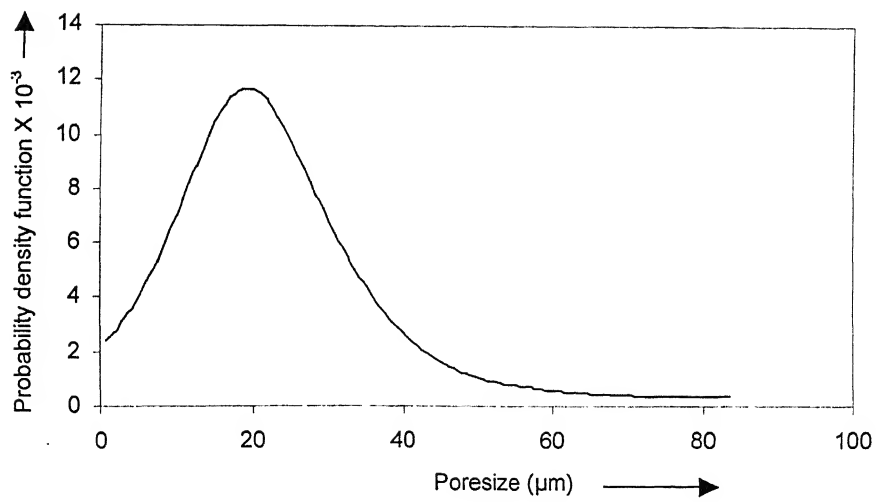


(d)

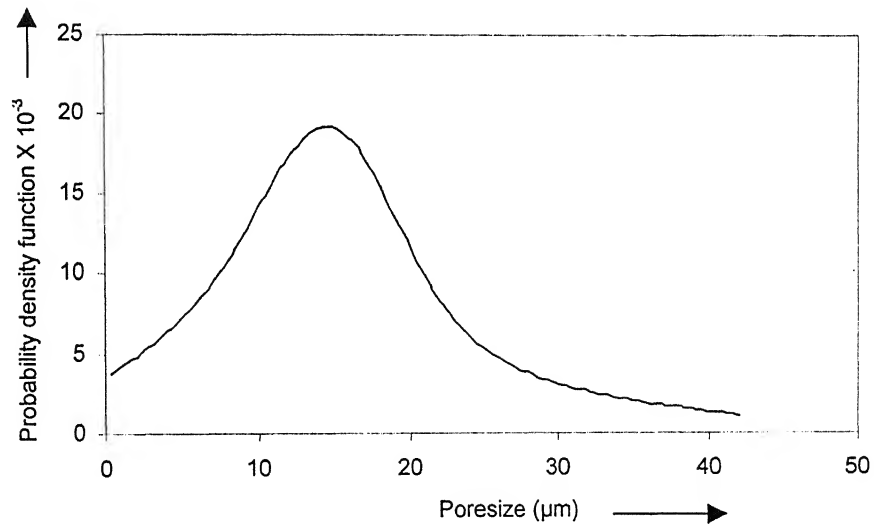
Figure 4.16. Pore Size Distribution Histogram for (a) 0%, (b) 20%, (c) 40% and (d) 60% Cold Rolling reduction.



(a)



(b)



(c)

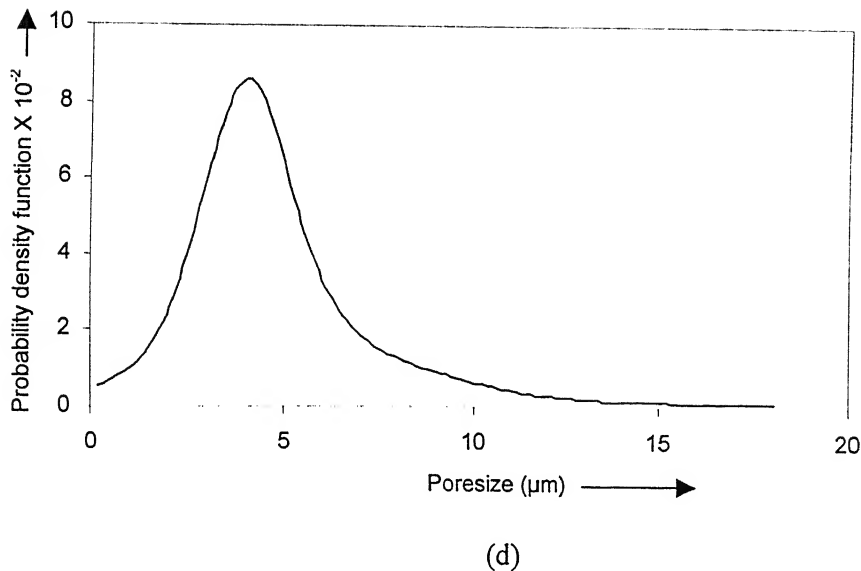


Figure 4.17. Pore size Probability distribution function on (a) 0%, (b) 20%, (c) 40% and (d) 60% Cold Rolling reduction. .

According to Figure 4.16 and Figure 4.17, at 0% cold rolling reduction pores are distributed in the size range from 4 μm to 90 μm , and the highest value of probability density function of pore size was observed at around 29 μm (75% pores are in the size range of 15 μm to 35 μm).

At 20 % cold rolling reduction, Number of big pores decrease and number of small pores was increased due to fragmentation of big pores in to smaller pores and the highest value of probability density function of pore size was observed at around 20 μm .

At 40 % cold rolling reduction, all pores bigger than 45 μm were eliminated and Number of smaller pores increased because of fragmentation of big pores and the highest value of probability density function of pore size was observed at around 15 μm .

At 60 % cold rolling reduction, most of the remaining were observed in the size range of 1 μm to 5 μm (75% pores having pore size smaller than 5 μm) and very few pores occur in the size range of bigger than 15 μm and all the pores bigger than 25

μm were eliminated and the highest value of pore size density function was observed at around 4 μm .

CHAPTER 5

DISCUSSIONS

From the help of Figure 4.10 to Figure 4.15, we can draw the various quantitative properties with respect to relative density of the cold rolled strip.

5.1 Effect of relative density of the strip on average pore size

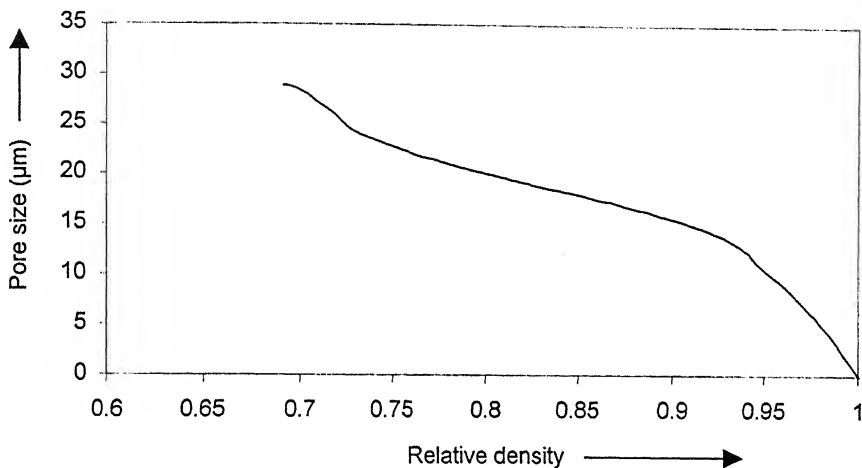


Figure 5.1. Changes in average pore size with the changes in relative density of strip

Average size of pores continuously decreases with increase in relative density of the strip as shown in Figure 5.1. Initial relative density of the strip is 0.69 at 0% cold rolling reduction. Initial (at relative density 0.69) Average pore size is 29 micron. At the Initial stage up to relative density of 0.72 decrease in average pore size at a higher rate was observed due to fragmentation of pores. After that average pore size decrease at a constant rate till relative density of 0.97. At these stages fragmentation and patching of pores both occurs simultaneously. After that

again decrease in average poresize occurs at a faster rate because of patching of pores only. No fragmentation occurs at these stages.

5.2 Effect of relative density of the strip on surface area of pores per unit volume

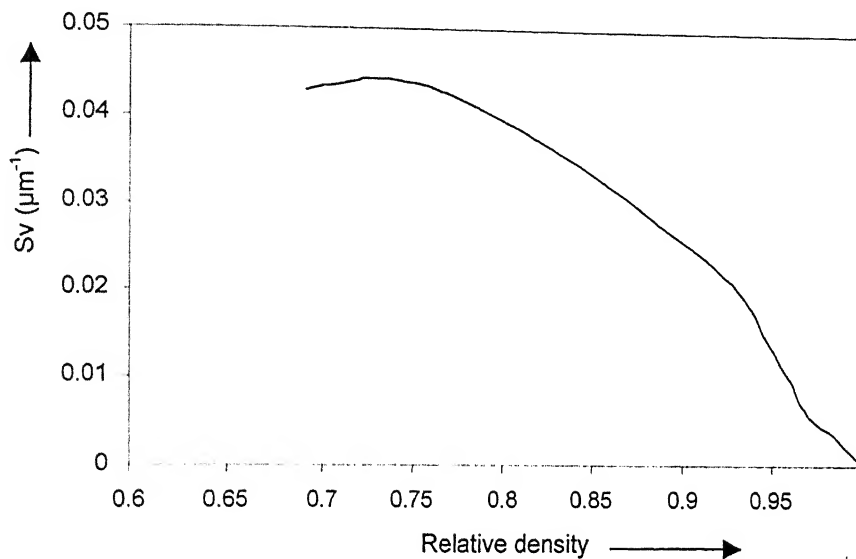


Figure 5.2. Changes in surface area of pores per unit volume with the changes in relative density of strip

At the initial stage up to relative density of 0.72 increases in surface area of pores per unit volume was observed because of elongation and fragmentation of pores. After that surface area of pores per unit volume decrease at a constant rate till relative density of 0.97. At these stages fragmentation and patching of pores both occurs simultaneously. After this stage (relative density of 0.97) surface area of pores per unit volume increase at a higher rate because of patching of pores only.

5.3 Effect of relative density of strip on aspect ratio of pores

Initially up to 0.72 relative density of strip, aspect ratio of pores increase with increase in relative density of strip because of fragmentation of big pore of lower aspect ratio in to smaller pores of higher aspect ratio. After that decrease in aspect ratio of pores was observed up to 0.85 relative density of the strip due to fragmentation of big pores of higher aspect ratio in to smaller pores of lower aspect ratio. After that increase in aspect ratio of pores up to relative density of 0.9 at a higher rate was observed because of patching of the fragmented pores. After these stages continuous decrease in aspect ratio of pores was observed and finally decreases to aspect ratio of 1 because of fragmentation of remaining bigger pores.

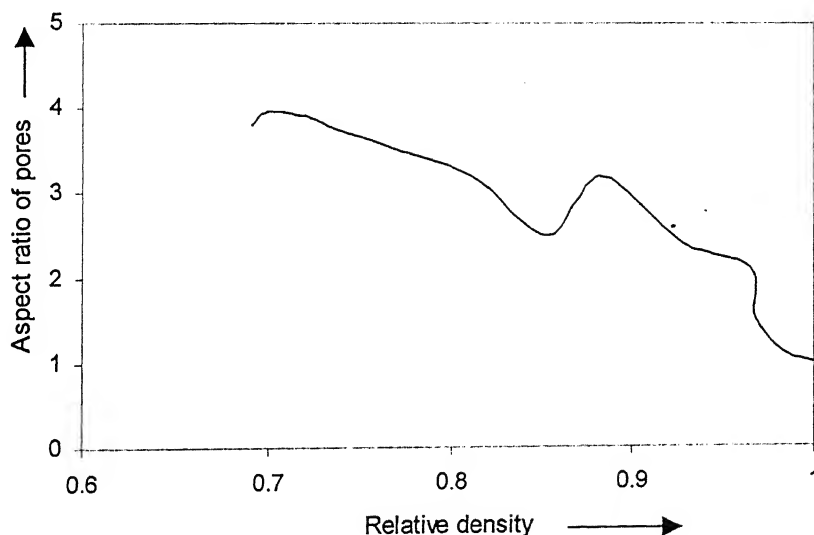


Figure 5.3. Changes in aspect ratio of pores with the changes in relative density of strip

5.4 Effect of relative density of strip on aspect ratio of grains

Aspect ratio of grains continuously increases with increase in relative density of the strip according to Figure 5.4. Increase in aspect ratio of grains was observed due to elongation of pores by rolling pressure. At the later stage after 0.97 relative density of the strip fast increase in aspect ratio was observed because of very less volume

fraction pores. At the later stage reason of fast change in aspect ratio of grains is that larger part of the rolling pressure are used in elongating the grains

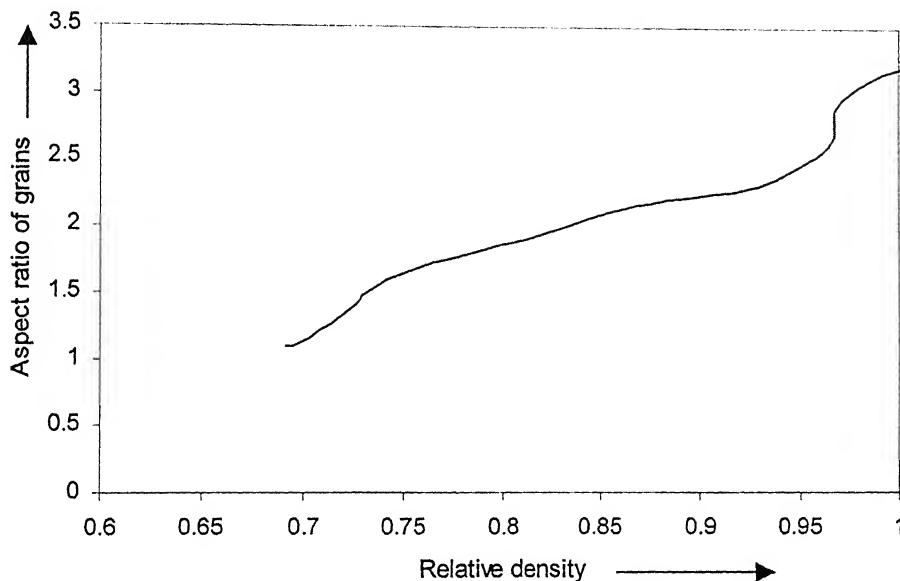


Figure 5.4. Changes in aspect ratio of grains with the changes in relative density of strip

5.5 Effect of relative density of strip on contiguity

There was no change in Contiguity of solid-solid contact till 0.71 relative density of the strip as shown in Figure 5.5. After that up to 0.97 relative densities increase in Contiguity at a constant rate with increase in relative density was observed due to fragmentation and patching of pores. After 0.97 relative density of strip fast increase in contiguity ratio was observed because of only patching is occur at these stages.

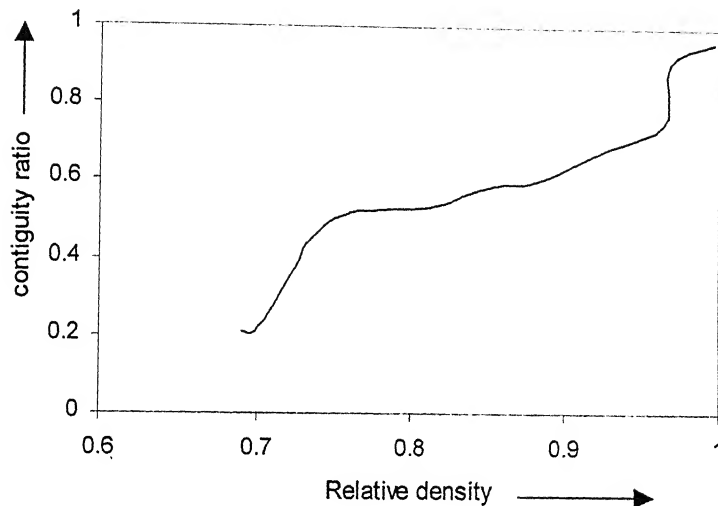


Figure 5.5. Changes contiguity ratio of solid-solid contact with the changes in relative density of strip

From all the above discussions it was observed that at the initial stage big pores are fragmented in to small pores and very less pores have patched up. Figure 4.16 and Figure 4.17 shows that percentage number of small pores increases as the % cold rolling reductions increases. Figure 4.13 and Figure 4.14 shows that till 20 % cold rolling reductions, aspect ratio of pores is not affected much because of fragmentation of very big pores in to smaller pores and patching of that fragmented pore and therefore there is decrease in average size of pores but there is no much change in aspect ratio of pores. From Figure 4.11 it was observed that surface area of pores per unit volume is increases till 20% cold rolling reductions due to fragmentation of big pores and very less patching of pores. Contiguity is also increases in this region due to fragmentation and patching of pore.

In the region between 20 % and 50 % cold rolling reduction, there was decrease in volume fraction of pores at a higher rate. In this region pores were patched up at a higher rate therefore decrease in surface area of pores per unit volume was observed. Average pores size was also decreasing in this region due to patching of pores.

In the region between 50% to 65% cold rolling reductions, there was decrease in volume fraction of pores at a lower rate due to patching of pores were more difficult in this region. Surface area of pores per unit volume was also decreases at a lower rate because of the same reason.

Over all process can be divided in three regions in first region fragmentation of pores is the dominant mechanism. Patching of pores occurs very less in this region. In the second region patching of pores and fragmentation of pores are occur at a higher rate. In the third region patching of pores is the main mechanism. Same result was observed from Figure 5.1 to Figure 5.5.

The reason of discrepancy in aspect ratio of pores was observed due to complexity of the process. After 15 % cold rolling reduction aspect ratio of pores decrease due to fragmentation of pores and after 35% cold rolling reduction there is an increase in aspect ratio because of elongation of the fragmented pores. After 40% cold rolling reduction aspect ratio of pores decrease with increase in % cold rolling reduction due to fragmentation of the elongated pores.

Conformance with the Koval'chenko equation

A quantitative relationship between the relative density and the coefficient of compression in hot rolling of porous strip has been derieved by Koval'chenko which can be written as fallows:

$$e_x = 1 - \left[\left(\frac{\rho_0}{\rho} \right)^{\frac{3m+1}{3m}} \left(\frac{1-\rho}{1-\rho_0} \right)^{\frac{1}{3m}} \right] \quad (5.1)$$

e_x = Fractional thickness deformation

ρ_0 = Relative density of starting strip (at 0% Cold Rolling Reduction)

ρ = Relative density of strip

m = Material constant

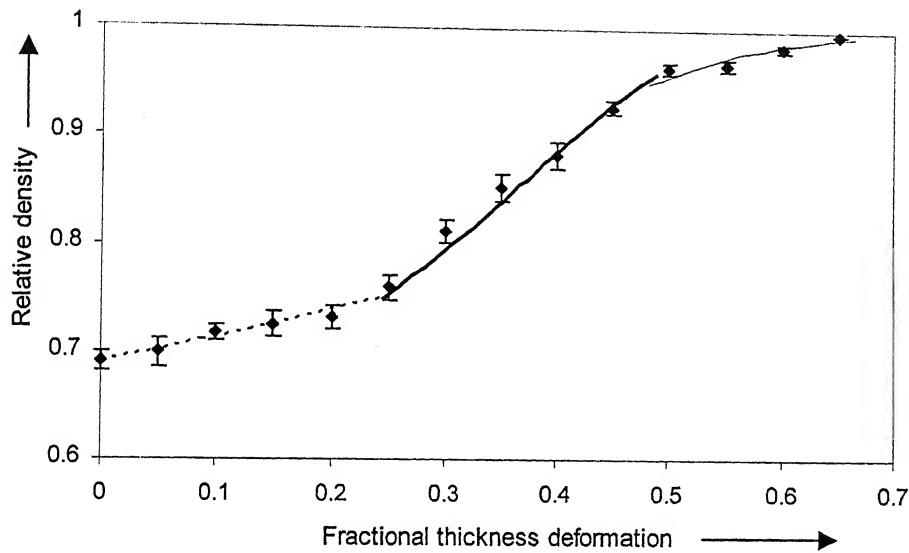


Figure 5.6. Comparison of experimental data with the data obtained from equation 5.1.

Figure 5.6 shows the comparison between the data obtained from the experiments and the data obtained from the equation 5.1.

In Figure 5.6, dots shows the experimental results and, three lines (dotted line, bold line and thin line) representing the equation 6 for $m=0.5$, $m=5.0$, and $m= 2.0$ respectively. There exists conformance at Initial region (0.0 to 0.25 fractional thickness deformation) between the experimental data and value derieved from the equation 5.1 for $m=0.5$. Similarly at the mid-region (0.25 to 0.48 fractional thickness deformation) and at the end region there exists conformance between the experimental data and value derieved from the equation 6 for $m=5.0$ and $m=2.0$ respectively.

This shows that value of m is not a constant at all the cold rolling deformation for a particular material. Value of m depends on the fractional thickness deformation of the metal strip.

CHAPTER 6

CONCLUSIONS

Considering results and discussions of the present investigation, the following conclusions can be drawn:

1. Densification process of porous metal strip can be divided in to three stages; in first stage fragmentation of pores is the dominant mechanism. Patching of pores occurs very less in this stage. In the second stage patching of pores and fragmentation of pores are occur at a higher rate. In the third stage patching of pores is the main mechanism.
2. Full densification was obtained at 65 % cold rolling reduction for a Ni metal strip produced by cold compaction fallowed by sintering (Initial relative density was 0.69 after sintering).
3. The value of material constant m in the Koval'chenko equation is not a constant at all the cold rolling deformation for a particular material. Value of m depends on the fractional thickness deformation of the metal strip.

CHAPTER 7

SUGGESTIONS FOR FUTURE WORK

The following are being the suggestions for future work in this area:

1. A more extensive study of the densification process of porous metal strip is required with respect to the amount of cold rolling reduction. Densification process should be studied in changes in internal structure of the metal strip for the smaller interval for % cold rolling reductions.
2. Stereological study of the densification process should be done for different initial relative densities of the Ni strip.
3. Stereological study of the densification process should be studied for hot rolling.

Appendix A

The Commonly used techniques for volume fraction analysis are based on one or more of the following principals:

1. **For an areal or Delesse analysis:** That the areal fraction of three-dimensional feature intercepted by random plane provides an unbiased estimate of the volume fraction of that feature.
2. **For a linear or Rosiwal analysis:** That the fractional intercept on a line passing at random through a two- or three-dimensional feature provides an unbiased estimate of, respectively, the areal or volume fraction of that feature.
3. **For a point-count analysis:** That the fractional number of randomly or regularly dispersed points falling within the boundaries of a two-dimensional feature on a plane, or within the boundaries of a three-dimensional feature in volume, provides an unbiased estimate of, respectively, the areal or volume fraction of that feature.

The absence of bias referred to in these principles does not, of course, imply that the results of an analysis will be free of error, but only that the expected result is equal to the true one.

Applications of the foregoing principles provide the following six possible experimental procedures:

a) Areal Analysis

This involves the measurement with a planimeter of the area of a constituent intercepted by plane of polish. In the assumed absence of experimental error, the only contribution to the variance of an areal measurement arises in the selection of a subarea for analysis from the plane of polish.

$$\left(\frac{\sigma_{A_f}}{\bar{A}_f} \right)^2 = \left(\frac{1}{M_a} \right) \left[\left(\frac{\sigma_a}{\bar{a}} \right)^2 + 1 \right] \quad (\text{A.1})$$

Where \bar{a} is the expected value of the area of the individual α features and \bar{M}_α is the expected total number.

b) Two-Dimensional Random Point Count

In this procedure we use the random numbers to select coordinates for the points. In this procedure there are two contributions to the variance; one arises from the deviation of the areal fraction in a subarea from the true volume fraction, and the other is introduced by the use of point count in place of a direct measurement of the areal fraction.

$$\left(\frac{\sigma_{N_f}}{\bar{N}_f} \right)^2 = \left(\frac{1}{\bar{N}_p} \right) \left(1 - \bar{A}_f \right) + \left(\frac{1}{\bar{M}_\alpha} \right) \left[\left(\frac{\sigma_\alpha}{\bar{a}} \right)_\alpha^2 + 1 \right] \quad (\text{A.2})$$

The first term in this equation is just the relative variance of a point count on a subarea having an areal fraction \bar{A}_f , and the second term is the variance in sampling for the subarea.

c) Two-Dimensional Systematic Point Count

In this procedure we use the points that are distributed in a prescribed manner. This procedure is easier than that of random point count method.

i) Coarse- Mesh Lattice

Here, for randomly dispersed features, the variance of the analysis is independent of their size distribution.

$$\left(\frac{\sigma_{N_f}}{\bar{N}_f} \right)^2 = \left(\frac{1}{\bar{N}_p} \right) \quad (\text{A.3})$$

ii) Fine- Mesh Lattice

$$\left(\frac{\sigma_{Nf}}{\bar{N}_f} \right)^2 < \left(\frac{1}{\bar{N}_p} \right) \left(\frac{0.15 \bar{l} d}{\bar{a}} \right) \left(\frac{1}{\bar{M}_a} \right) \left[\left(\frac{\sigma_a}{\bar{a}} \right)^2 + 1 \right] \quad (\text{A.4})$$

where \bar{l} is the expected perimeter length of the α features and \bar{M}_a is the expected number of features and \bar{N}_p the expected number of points that they occupy.

d) Linear Analysis

A measurement of the fractional line length intercepted. It is usually performed by traversing the specimen under the cross hairs of a microscope and recording the distance traveled in each constitute.

$$\left(\frac{\sigma_{L_f}}{\bar{L}_f} \right)^2 = \left(\frac{1}{\bar{M}_t} \right) \left(1 - \bar{L}_f \right)^2 \left[\left(\frac{\sigma_t}{\bar{t}} \right)^2 + \left(\frac{\sigma_t}{\bar{t}} \right)^2 \right] \quad (\text{A.5})$$

e) One-Dimensional Random Point Count

Instead of measuring the lineal fraction directly, it can be estimated by distributing points at random along a transverse, and counting the fraction falling on α features.

$$\left(\frac{\sigma_{Nf}}{\bar{N}_f} \right)^2 = \left(\frac{1}{\bar{N}_p} \right) \left(1 - \bar{L}_f \right) + \left(\frac{1}{\bar{M}_t} \right) \left(1 - \bar{L}_f \right)^2 \left[\left(\frac{\sigma_t}{\bar{t}} \right)^2 + \left(\frac{\sigma_t}{\bar{t}} \right)^2 \right] \quad (\text{A.6})$$

f) One-Dimensional Systematic Point Count

i) Coarse- Mesh Lattice

$$\left(\frac{\sigma_{Nf}}{\bar{N}_f} \right)^2 = \left(\frac{1}{\bar{N}_p} \right) \quad (\text{A.7})$$

ii) Fine- Mesh lattice

$$\left(\frac{\sigma_{N_f}}{\bar{N}_f} \right)^2 \leq \left(\frac{1}{\bar{N}_p} \right) \left(\frac{d}{4t} \right) + \left(\frac{1}{\bar{M}_t} \right) \left[\left(\frac{\sigma_t}{t} \right)^2 + 1 \right] \quad (\text{A.8})$$

From these equation Hilliard and Cahn [39] have concluded that the best method for volume fraction analysis is a systematic point count in which a grid is superimposed on a sequence of areas selected either randomly or systematically from the plane of polish. The total fraction of grid corners falling on a particular phase provides a unbiased estimate of the volume fraction of that phase.

Appendix B

95 % Confidence level

The 95 % confidence level tells us how sure we can be. It is expressed as a percentage and represents how often the true percentage of the population who would pick an answer lies within the confidence interval. The 95% confidence level means we can be 95% certain; the 99% confidence level means you can be 99% certain. Most researchers use the 95% confidence level.

$$95\% \text{ Confidence Limit} = \frac{ts}{(n-1)^{1/2}}$$

Where, n = number of measurements, and

$$s = \left(\frac{\sum (x_i - \bar{x})^2}{n-1} \right)^{1/2}$$

t value depends on the value of n-1.

REFERENCES

1. J. H. Tundermann and A. R. E. Singer, *Powder Metall.*, 1968, 11, pp. 261-294.
2. P. E. Evans, in 'New methods for the consolidation of metal powders', (ed. H. H. Hausner), pp. 99-118; 1967, New York, Plenum Press.
3. P. E. Evans and G. C. Smith, *Powder Metall.*, 1959, (3), pp. 26-44.
4. V. S. Smirnov, N. N. Pavlov, and N. N. Tselesin, *Sov. Powder Metall. Met. Ceram.*, 1968, 6, pp. 441-443.
5. R. A. Smucker, *Iron Steel Eng.*, 1959, 36, (7), pp. 118-124.
6. G. M. Sturgeon and R. L. S. Taylor, 'Metal strip from powder', 46; 1972, London, Mills and Boon.
7. S. Bhargava and R. K. Dube, *Metall. Trans.*, 1988, 19A, (5), pp. 1205-1211.
8. M. S. Koval'Chenko, *Sov. Powder Metall. Met. Ceram.*, 1978, 17, pp. 351-356.
9. C. H. Weaver, R. G. Butters, and J. A. Lund, *Int. J. Powder Metall.*, 1972, 8, pp. 3-15.
10. T. Kimura, H. Hirabayashi, and M. Tokuyoshi, *Rev. Electr. Commun. Lab. (jpn)*, 1964, 12, pp. 341-354.
11. M. H. D. Blore, V. Silins, S. Romanchuk, T. W. Benz, and V. N. Mackiw, *Met. Engg. Q.*, 1966, 6, pp. 314-329.
12. R. W. Fraser, D. J. I. Evans, and V. N. Mackiw, *Cobalt*, 1964, (23), pp. 72-81.
13. A. F. Marshall, *Powder Metall.*, 1960, (5), pp. 24-31.
14. G. M. Sturgeon, G. Jackson, V. Barker, and G. M. H. Sykes, *Powder Metall.*, 1968, 11, pp. 314-329.
15. D. G. Hunt and R. Eborall, *Powder Metall.*, 1960, (5), pp. 1-23.
16. D. K. Worn and R. P. Perks, *Powder Metall.*, 1959, (3), pp. 45-71.
17. I. Davis, W. M. Gibbon, and A. G. Harris, *Powder Metall.*, 1968, 11, pp. 259-331.
18. S. Storchheim, *Met. Prog.*, 1956, 70, (3), pp. 120-126.

19. J. A. Lund, *J. Met.*, 1958, 10, (11), pp. 731-734.
20. S. Shima and M. Yamada, *Powder Metall.*, 1984, 27, pp. 39-44.
21. M. A. Clegg, M. J. H. Ruscoe, and R. W. Frasher, in 'Progress in powder metallurgy', Vol. 37, pp. 359-369: 1982, Princeton, NJ, Metal Powder Industry Federation.
22. J. H. Tundermann and A. R. E. Singer, *Powder Metall.*, 1969, 12, pp. 219-242.
23. P. E. Evans and G. C. Smith, in 'New methods for the consolidation of metal powders', (ed. H. H. Hausner), pp. 119-168; 1967, New York, Plenum Press.
24. R. S. Lee and E. G. Schwartz, *Int. J. powder Metall.*, 1967, 3, pp. 83-92.
25. 'Metals handbook'. 9 edn., vol. 7, pp. 402; 1984, Metals Park, OH, American Society of Metals.
26. R. K. Dube, *Powder Metall. Int.*, 1981, 13, pp. 188-190.
27. R. K. Dube, *Powder Metall. Int.*, 1983, 15, pp. 36-40.
28. A. R. E. Singer, *Met. Technol.*, 1974, 1, pp. 353-359.
29. A. R. E. Singer and R. K. Dube, *Trans. Indian Inst. Met.*, 1975, 28, pp. 131-137.
30. P. E. Evans and G. C. Smith, in 'Symposium on powder metallurgy 1954', pp. 131-136; 1956, London, The Iron and Steel Institute.
31. G. Naeser and F. Zirm, *Stahl, Stahl Eisen*, 1950, 70, pp. 995-1004.
32. Siemens and Halske, German Patent No. 154 998, Nov. 1904.
33. H.A. Kuhn and C.L. Downey. *Int. J. Powder Metall.* 7 (1971), pp. 5.
34. R.J. Green. *Int. J. Mech. Sci.* 14 (1972), p. 215.
35. S. Shima and M. Oyane. *Int. J. Mech. Sci.* 18 (1976), p. 285.
36. A. R. desmukh, T. Sundararajan, R.K. Dube, S. Bhargava, *J. of Material Processing Technology*, 84, 1998, pp. 56-72.
37. L.R. Underwood, *The Rolling of Metals* Vol. 1. Chanman and Hall, London, 1952, pp. 168-202.

38. Eustace C. Larke, *The Rolling of Strip, Sheet and Plate*, Chapman and Hall, London, 1957, pp. 174–202.

39. John E. Hilliard and John W. Cahn, *Transactions of The Metallurgical Society of AIME*, 221, april 1961, pp. 344-352.